

Broad bounds on Earth’s accretion and core formation constrained by geochemical models

John F. Rudge^{*1,2}, Thorsten Kleine^{1,3}, and Bernard Bourdon¹

¹Institute of Geochemistry and Petrology, ETH Zürich,
Clausiusstrasse 25, NW, 8092 Zürich, Switzerland.

²Institute of Theoretical Geophysics, Bullard Laboratories, University of Cambridge,
Madingley Road, Cambridge, CB3 0EZ, UK.

³Institut für Planetologie, Westfälische Wilhelms-Universität Münster,
Wilhelm-Klemm-Str. 10, 48149 Münster, Germany.

April 22, 2010

Prevailing models of Earth’s core formation based on hafnium-tungsten and uranium-lead chronometry imply a rapid early accretion of Earth’s main mass in ~ 10 Myr^{1–4}, followed by a moon-forming giant impact terminating accretion at either ~ 30 ^{1,5} or ~ 100 ^{2,3} Myr after solar system formation. These models assume full metal-silicate equilibration during core formation, consistent with the core-mantle partitioning of siderophile elements^{6,7}. Here we show that the geochemical observations permit a much wider range of possibilities, yet still provide bounds on Earth’s accretion and core formation. The Hf-W system mainly constrains the degree of core-mantle equilibrium rather than the accretion timescale, whilst the U-Pb system constrains Earth’s terminal accretion to ~ 4.45 billion years ago, consistent with the age of the Moon^{8,9}. Exploring a wide parameter space within geochemical models demonstrates that at least 36% of Earth’s core formed in equilibrium with the mantle. We conclude that both equilibrium and disequilibrium models are equally compatible with the geochemical observations, suggesting that a better understanding of the physical and chemical conditions of metal-silicate segregation is required to more tightly constrain Earth’s accretion.

Impacts of numerous Moon- to Mars-sized planetary embryos on the growing Earth released sufficient energy to induce melting and core formation within the Earth^{10,11}. As metal segregation is thought to happen much faster than accretion, the time scale of core formation can be used to determine the rate of Earth’s accretion. The Hf-W systematics of Earth’s mantle yield model time scales for accretion that are faster than those estimated based on U-Pb systematics. The equilibrium two-stage model ages are $t_{2,\text{eq}}^{\text{Hf-W}} = 31.0 \pm 4.4$ Myr^{4,12–14} and $t_{2,\text{eq}}^{\text{U-Pb}} = 55.9 - 130.5$ Myr. The model ages calculated in an exponential growth model are roughly a factor of 3 smaller, with $\tau_{a,\text{eq}}^{\text{Hf/W}} = 10.6 \pm 0.5$ Myr and $\tau_{a,\text{eq}}^{\text{U-Pb}} = 21.6 - 51.0$ Myr (τ_a corresponds to time taken to achieve 63% growth; the time to achieve 95% growth is similar to the two stage model ages) (Supplementary Methods). Several models were proposed to

account for this disparity in calculated accretion time scales, including disequilibrium during core formation^{15–17}, a late segregation of Pb-bearing sulphides to the Earth’s core^{18,19}, and the addition of Pb by a late veneer subsequent to core formation⁵. The main source of uncertainty in using Hf-W systematics to determine the core formation time scale is the strong dependence of the system on the degree of metal-silicate equilibration^{12,15–17}. Some authors have argued that U-Pb systematics place no constraint on core formation because neither the bulk Earth Pb isotopic composition nor the bulk Earth U/Pb ratio are sufficiently well known^{20,21}. Additional uncertainty arises because some recent experiments seem to indicate that Pb was not partitioned into the Earth’s core²², although this result has been questioned by others²³ due the high C contents of the metal phase in those experiments. In any case, the U-Pb age of the Earth appears to have some significance, because it is similar to the age of the Moon^{8,9}.

A serious shortcoming of current geochemical models of Earth’s accretion and core formation is that their entire parameter space has never been fully explored. For instance, all the models use specific growth curves without investigating the entire range of possible curves. It thus remains unclear whether the particular accretion curve chosen provides the best approximation of Earth’s accretion. Furthermore, existing models of disequilibrium^{15–17,24} have not studied the combined constraints of both isotopic and siderophile element observations. To address these important questions, we developed a geochemical box model for metal-silicate differentiation in the growing Earth. In the model, material of the planetary embryos is assumed to differentiate into mantle and core at time 0 (the time of solar system formation), with metal and silicate in equilibrium with one another. This assumption seems reasonable, given the evidence for very early differentiation of meteorite parent bodies^{12,25}. Over the course of the accretion, the embryo material is added to the Earth at some rate described by a function $M(t)$ which determines the fraction of the Earth that has accreted at time t . Two forms for $M(t)$ are commonly chosen: a step function (two stage model),

$$M(t) = \begin{cases} 0, & 0 < t < t_2, \\ 1, & t > t_2, \end{cases} \quad (1)$$

where all the accretion occurs at a particular instant t_2 ; or an exponential

$$M(t) = 1 - e^{-t/\tau_a}, \quad (2)$$

which has similarities with the accretion curves produced by some n -body simulations^{26,27}. τ_a is the corresponding mean age. A useful two parameter generalisation of the exponential accretion model is the Weibull accretion model,

$$M(t) = 1 - e^{-(t/\alpha)^\beta}, \quad (3)$$

where α is a time scale parameter (time taken to accrete 63% of the Earth), and β is a shape parameter. When $\beta < 1$ accretion happens faster than exponential at early times, and slower than exponential at late times.

As accretion proceeds, material from the mantle of the embryos is added directly to the Earth’s mantle. However, a mass fraction k of material from the core of the embryos chemically equilibrates with the Earth’s mantle before joining the Earth’s core, with the remaining fraction $1 - k$ added directly to the Earth’s core. When $k = 1$, the model is an equilibrium

model, and all memory of differentiation in the embryos is lost. For $k < 1$ there will be some memory of the embryos' differentiation. k represents a simple parametrisation of the complex interactions that take place between metal and silicate during accretion. The degree of metal-silicate equilibration depends crucially on the physical conditions under which metal-silicate segregation takes place¹⁰. For example, in a turbulently convecting magma ocean the metal may fall through the liquid silicate as small droplets, equilibrating in the process. But it is unclear whether the metal cores of newly accreted objects always emulsify in this way, and some cores may have directly merged with Earth's core without substantial metal-silicate equilibration.

The chemical equilibration processes that take place both in the embryos and during Earth's accretion are described by metal/silicate partition coefficients D , which are functions of the temperature, pressure and oxygen fugacity conditions under which chemical equilibration takes place. Thus, the partitioning is likely to have changed dramatically over the course of Earth's accretion. We model this with the approach used by Wade and Wood⁶. The point of last metal-silicate equilibration is assumed to be at the base of a magma ocean, which is at some fixed fraction of the depth to the core-mantle boundary. Thus as the planet grows, the pressure at the base of the magma ocean increases. The temperature at the base of the magma ocean is simply a function of this pressure, set by the constraint that it lies on the peridotite liquidus, and also increases as the Earth grows. The oxygen fugacity is also assumed to evolve over the course of the accretion, linearly increasing with $M(t)$ after the first 10% of the accretion⁷. Using parametrisations of experimental data on metal-silicate partitioning^{6,28-30}, the expected siderophile element depletion of the mantle due to core formation can be calculated.

In agreement with earlier work, models with full equilibration ($k = 1$) can produce good fits to the observed siderophile element abundances (Figure 1a), and require an increase in oxygen fugacity of around 3 log units over the course of accretion^{6,7}. However, equally good fits can be found in scenarios with partial equilibration, as shown in Figure 1b. Thus, the siderophile element depletions in Earth's mantle are not evidence for equilibrium core formation and consequently cannot be used to argue for complete metal-silicate equilibration when interpreting the isotopic observations. In partial equilibration scenarios, the conditions of differentiation in the embryos are important, and these are very poorly constrained. There is a trade off between conditions in the embryos and conditions on Earth, and good fits can be found for a wide range of different embryo conditions (Supplementary Methods). Thus, the siderophile element abundances may reflect not only the conditions of core formation in the growing Earth but also the conditions of core formation in the embryos.

Whilst the dramatic changes in partitioning behaviour over the course of accretion are key to understanding the siderophile element abundances, the main constraints that the isotopic observations place can be understood within the context of simpler constant partitioning models. Such a model can be seen in Figure 2, which shows an equilibrium Weibull accretion model of the Earth with the values of α and β compatible with the Hf-W and U-Pb observations, assuming constant partitioning. There is a region of overlap around $\alpha = 0.4 - 2.5$ Myr, $\beta = 0.22 - 0.36$ where the two isotopic systems are consistent. Thus, having a rapid accretion at early times (63% of the Earth accreted in less than 2.5 Myr) and a slower accretion at late times is one way to match the isotopic observations with an equilibrium model. Thus, the apparent disparity between the previously calculated Hf-W and U-Pb time scales for Earth's accretion may simply reflect the choice of an improper accretion curve (i.e. the

exponential or two stage models) rather than being a case for partial equilibration^{15,17}, late sulphide segregation¹⁹, or late veneer Pb addition⁵.

A key unknown in interpreting the isotopic observations is the degree of metal-silicate equilibration during core formation. This is demonstrated in Figure 3b, where the two stage age t_2 is given as a function of k for both Hf-W and U-Pb. Importantly, there is a region of overlap $k = 0.36 - 0.41$ and $t_2 = 67.1 - 162.9$ Myr where both systems are consistent. The exponential model ages (shown in Figure 3a) also overlap, with $k = 0.37 - 0.42$ and $\tau_a = 33.9 - 85.8$ Myr. As can be seen by the flattening of the curves in Figure 3 for large τ_a and t_2 for Hf-W, there is a minimum amount of equilibration required to be compatible with the observations. This minimum value is the same for any accretion curve, and is determined by the Hf-W observations to be in the range $k = 0.36 - 0.39$. For both two stage and exponential models, the amount of equilibration required to get a match between Hf-W and U-Pb is very close to this lower bound. Hf-W thus provides very little information about the timing of accretion in such models, and essentially determines the degree of equilibration. U-Pb is less sensitive to the degree of equilibration and mostly determines the timing¹⁷.

The discussion up to this point illustrates that a variety of different accretion scenarios are compatible with the observations. Nevertheless the observations still place important constraints. Isotopic observations only fully determine the accretion curve $M(t)$ when simple parametric forms are assumed, such as an exponential model or a two stage model. In general, $M(t)$ will be underconstrained, but there are bounds that can be placed on $M(t)$ which are shown as pink (Hf-W) and green (U-Pb) shaded regions in Figure 4. Slightly tighter bounds are obtained when both Hf-W and U-Pb constraints are considered together (yellow region). Accretion curves compatible with the observations must lie wholly within the unshaded region.

The shaded regions shown in Figure 4a provide a clear demonstration of the different constraints the Hf-W and U-Pb systems place on equilibrium accretion. Hf-W predominately constrains the early accretion, e.g. it shows that at least 80% of the Earth must have accreted by 35 Myr; but it tells us very little about the late (> 60 Myr) accretion other than that no more than 14% of the accretion can happen late: as far as the Hf-W observations are concerned the last 14% of the accretion could have happened yesterday. On the other hand, U-Pb tells us little about the early accretion, but strongly constrains the late accretion, e.g. it shows that the final 10% of accretion must have begun by 120 Myr for the assumed parameters. The bounds on the accretion curve depend on the degree of equilibration, and Figure 4b gives an example with partial equilibration.

In summary, we can simultaneously match both the siderophile element abundances and the isotopic constraints with a single model. However, there are a wide range of models, both equilibrium and disequilibrium, that are all equally compatible with the observations. Based on the Hf-W, U-Pb, and siderophile element constraints we cannot tell whether full core-mantle equilibration occurred or not, but we can constrain the degree of equilibration to be at least 36%. Thus, in spite of a wide range of geochemical observations, important details regarding Earth's accretion and core formation remain only poorly constrained. A better understanding of the physical and chemical conditions of metal-silicate fractionation as well as of the conditions prevailing in Earth's building blocks are needed before more tightly defined accretion curves for the Earth can be constructed.

Methods Summary

The geochemical box model used throughout this work is governed by

$$\frac{d}{dt} ((1 - F)M c_m) = [(1 - F) c_{me} + kF (c_{ce} - D_c c_m)] \frac{dM}{dt}, \quad (4)$$

$$\frac{d}{dt} (FM c_c) = [kF D_c c_m + (1 - k)F c_{ce}] \frac{dM}{dt}, \quad (5)$$

where $F = 0.323$ is the mass fraction of Earth that is core, k is the mass fraction of metal that equilibrates during accretion, D_c is the metal/silicate partition coefficient, c_m is the concentration of a chemical species in Earth's mantle, c_c is the concentration in Earth's core, c_{me} is the concentration in the mantle of the embryos, c_{ce} is the concentration in the core of the embryos, and $M(t)$ is the fraction of the Earth that has accreted at time t .

The parameter k is a simple representation of the equilibration of the metal as it travels through the Earth's mantle to the core, and models the equilibration process as a simple mixture of fully equilibrated and unequilibrated material. The real situation may be more complicated, as different elements have different diffusivities and thus may equilibrate at different rates. Hence the effective k could differ between different elements. For simplicity we treat k as a constant for all elements.

If the partition coefficients vary with time then the governing equations have to be solved numerically (Figure 1). The partition coefficients are a function of temperature, pressure, and oxygen fugacity and have been parametrised using regressions of experimental data^{6,7,28–30}. There are uncertainties in the regression coefficients and these have been propagated through the model to generate the red error bars shown in Figure 1. It should be noted that these red error bars may underestimate or overestimate the true uncertainty for two main reasons: First, errors have only been included on some of the regression coefficients used in the parametrisation. If errors were included on all of the regression coefficients then the error bars would be substantially larger³⁰, but not all authors report errors on all coefficients. Second, the errors on the regression coefficients have been assumed to be independent, so the true uncertainty could be larger or smaller depending on the degree of correlation between the regression coefficients, but this correlation is not reported. There are also uncertainties in the present day mantle abundances, and these are shown in the blue error bars of Figure 1.

A number of simple analytical results arise when the partitioning is constant, as assumed in Figures 2–4. Detailed derivations of the following results can be found in the Supplementary Methods. The two stage ages with (t_2) and without ($t_{2,eq}$) disequilibrium are related by

$$1 - e^{-\lambda t_{2,eq}} = \frac{k(1 + R_d)}{1 + kR_d} (1 - e^{-\lambda t_2}), \quad (6)$$

where λ is the decay constant and $R_d = FD_d/(1 - F)$. D_d is the (assumed constant) metal/silicate partition coefficient of the daughter element (W or Pb). This is the relationship plotted in Figure 3b.

The two stage model ages t_2 and the exponential model ages τ_a are related by

$$e^{-\lambda t_2} = \frac{\Gamma(2 + kR_d)\Gamma(1 + \lambda\tau_a)}{\Gamma(2 + kR_d + \lambda\tau_a)}, \quad (7)$$

where $\Gamma(z)$ is the Gamma function, and this is used in plotting Figure 3a.

A lower bound on k is given by

$$k \geq \frac{1 - e^{-\lambda t_2, \text{eq}}}{1 + R_d e^{-\lambda t_2, \text{eq}}}, \quad (8)$$

and this describes the asymptotes for large t_2 and τ_a in [Figure 3](#).

The early accretion ($t \leq t_2$) is bounded by (pink and green regions, upper left of [Figure 4](#))

$$M(t) \leq e^{\lambda(t-t_2)/(1+kR_d)}, \quad (9)$$

and the late accretion ($t \geq t_2$) by (pink and green regions, lower right of [Figure 4](#))

$$M(t) \geq \left(\frac{e^{-\lambda t_2} - e^{-\lambda t}}{1 - e^{-\lambda t}} \right)^{1/(1+kR_d)}. \quad (10)$$

The isotopic evolution of models with evolving partitioning behaviour, such as those in [Figure 1](#), do not differ substantially from the constant partition coefficient models of [Figures 2, 3, and 4](#). The only difference is that accretion needs to be slightly more protracted to match the same Hf-W and U-Pb observations. The requirement of more protracted accretion arises because both W and Pb are more siderophile during the early accretion than the late accretion, which causes a bias towards younger ages. For example, the disequilibrium model of [Figure 1b](#) (evolving partitioning) requires an exponential accretion with $\tau_a = 49.7$ Myr and $k = 0.42$ as opposed to $\tau_a = 40.3$ Myr and $k = 0.40$ of [Figure 4b](#) (constant partitioning).

References

- [1] Jacobsen, S. B. The Hf-W isotopic system and the origin of the Earth and Moon. *Annu. Rev. Earth Planet. Sci.* **33**, 531–570 (2005).
- [2] Halliday, A. N. A young Moon-forming impact at 70-110 million years accompanied by late-stage mixing, core formation and degassing of the Earth. *Phil. Trans. R. Soc. A* **366**, 4163–4181 (2008).
- [3] Halliday, A. N. & Wood, B. J. How did Earth accrete? *Science* **325**, 44–45 (2009).
- [4] Yin, Q. *et al.* A short timescale for terrestrial planet formation from Hf-W chronometry of meteorites. *Nature* **418**, 949–952 (2002).
- [5] Albarède, F. Volatile accretion history of the terrestrial planets and dynamic implications. *Nature* **461**, 1227–1233 (2009).
- [6] Wade, J. & Wood, B. J. Core formation and the oxidation state of the earth. *Earth Planet. Sci. Lett.* **236**, 78–95 (2005).
- [7] Corgne, A., Keshav, S., Wood, B. J., McDonough, W. F. & Fei, Y. Metal-silicate partitioning and constraints on core composition and oxygen fugacity during Earth accretion. *Geochim. Cosmochim. Acta* **72**, 574–589 (2008).
- [8] Touboul, M., Kleine, T., Bourdon, B., Palme, H. & Wieler, R. Late formation and prolonged differentiation of the Moon inferred from W isotopes in lunar metals. *Nature* **450**, 1206–1209 (2007).

- [9] Touboul, M., Kleine, T., Bourdon, B., Palme, H. & Wieler, R. Tungsten isotopes in ferroan anorthosites: Implications for the age of the Moon and lifetime of its magma ocean. *Icarus* **199**, 245–249 (2009).
- [10] Rubie, D. C., Nimmo, F. & Melosh, H. J. Formation of Earth’s Core. In *Treatise on Geophysics* (Elsevier, 2007).
- [11] Stevenson, D. J. Earth formation and evolution. In *Treatise on Geophysics*, 1–11 (Elsevier, 2007).
- [12] Kleine, T. *et al.* Hf-W chronology of the accretion and early evolution of asteroids and terrestrial planets. *Geochim. Cosmochim. Acta* **73**, 5150–5188 (2009).
- [13] Kleine, T., Münker, C., Mezger, K. & Palme, H. Rapid accretion and early core formation on asteroids and the terrestrial planets from Hf-W chronometry. *Nature* **418**, 952–955 (2002).
- [14] Schoenberg, R., Kamber, B. S., Collerson, K. D. & Eugster, O. New W-isotope evidence for rapid terrestrial accretion and very early core formation. *Geochim. Cosmochim. Acta* **66**, 3151–3160 (2002).
- [15] Halliday, A. N. Mixing, volatile loss and compositional change during impact-driven accretion of the Earth. *Nature* **427**, 505–509 (2004).
- [16] Kleine, T., Mezger, K., Palme, H. & Münker, C. The W isotope evolution of the bulk silicate Earth: constraints on the timing and mechanisms of core formation and accretion. *Earth Planet. Sci. Lett.* **228**, 109–123 (2004).
- [17] Allègre, C. J., Manhès, G. & Göpel, C. The major differentiation of the Earth at ~ 4.45 Ga. *Earth Planet. Sci. Lett.* **267**, 386–398 (2008).
- [18] Halliday, A. N. & Wood, B. J. The composition and major reservoirs of the Earth around the time of the Moon-forming giant impact. In *Treatise on Geophysics* (Elsevier, 2007).
- [19] Wood, B. J. & Halliday, A. N. Cooling of the Earth and core formation after the giant impact. *Nature* **437**, 1345–1348 (2005).
- [20] Kamber, B. S. & Kramers, J. D. How well can Pb isotopes date core formation? *Nature* **444**, E1–2 (2006).
- [21] Yin, Q. & Jacobsen, S. B. Does U-Pb date Earth’s core formation? *Nature* **444**, E1 (2006).
- [22] Lagos, M. *et al.* The Earth’s missing lead may not be in the core. *Nature* **456**, 89–92 (2008).
- [23] Wood, B. J. & Halliday, A. N. Lead was strongly partitioned into Earth’s core and not lost to space. *Geochim. Cosmochim. Acta* **73**, A1451 (2009). 19th Annual V.M. Goldschmidt Conference, Davos, Switzerland.
- [24] Wänke, H. Constitution of terrestrial planets. *Phil. Trans. Roy. Soc. A* **303**, 287–302 (1981).

- [25] Kleine, T., Mezger, K., Palme, H., Scherer, E. & Münker, C. Early core formation in asteroids and late accretion of chondrite parent bodies: Evidence from $^{182}\text{Hf} - ^{182}\text{W}$ in CAIs, metal-rich chondrites, and iron meteorites. *Geochim. Cosmochim. Acta* **69**, 5805–5818 (2005).
- [26] Wetherill, G. W. Accumulation of the terrestrial planets and implications concerning lunar origin. In Hartmann, W. K., Philips, R. J. & Taylor, G. J. (eds.) *Origin of the Moon*, 519–550 (Lunar Planetary Institute, Houston, 1986).
- [27] Raymond, S. N., Quinn, T. & Lunine, J. I. High-resolution simulations of the final assembly of Earth-like planets I. Terrestrial accretion and dynamics. *Icarus* **183**, 265–282 (2006).
- [28] Wood, B. J., Nielsen, S. G., Rehkämper, M. & Halliday, A. N. The effects of core formation on the Pb- and Tl- isotopic composition of the silicate Earth. *Earth Planet. Sci. Lett.* **269**, 326–336 (2008).
- [29] Wood, B. J., Wade, J. & Kilburn, M. R. Core formation and the oxidation state of the Earth: Additional constraints from Nb, V and Cr partitioning. *Geochim. Cosmochim. Acta* **72**, 1415–1426 (2008).
- [30] Cottrell, E., Walter, M. J. & Walker, D. Metal-silicate partitioning of tungsten at high pressure and temperature: Implications for equilibrium core formation in Earth. *Earth Planet. Sci. Lett.* **281**, 275–287 (2009).

Author Information

Correspondence and requests for material should be addressed to J. F. Rudge (rudge@esc.cam.ac.uk).

Acknowledgements

We thank A. Corgne, J. Wade, M. Walter, and B. Wood for discussions, and F. Albarède for his review.

Competing Financial Interests

The authors declare no competing financial interests.

Author Contributions

J.R. derived the model equations and performed the calculations. J.R. and T.K. wrote the paper. B.B. conceptually designed the study. All authors discussed the results and implications and commented on the manuscript.

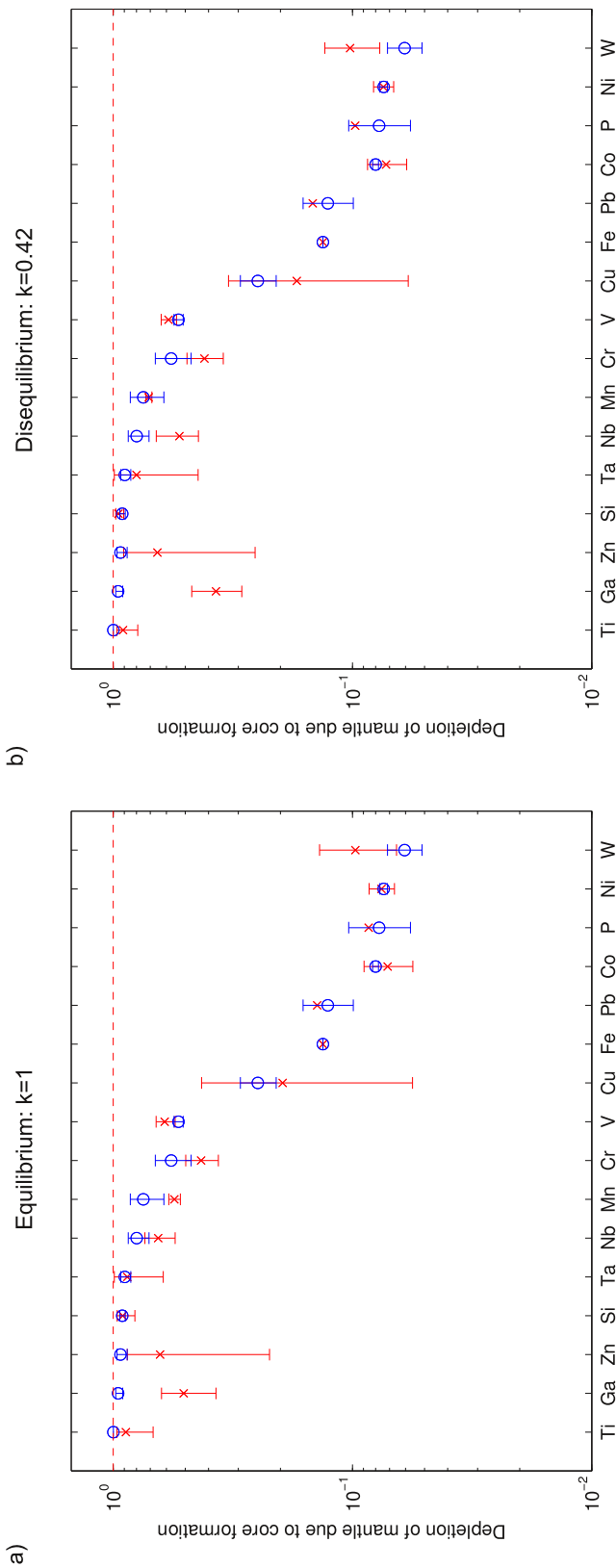


Figure 1: Present day mantle depletion for a variety of moderately siderophile elements. Blue dots give target values^{6,7}, red crosses give model results using experimental partition coefficients^{6,7,29,30}. Error bars give 1σ uncertainties. a) is an equilibrium scenario ($k = 1$), where oxygen fugacity increases from $\Delta JW = -4.26$ to -0.83 . The pressure of equilibration is 31% of that at the core-mantle boundary. b) is a disequilibrium scenario ($k = 0.42$), where oxygen fugacity increases from $\Delta JW = -2.62$ to -0.57 , and the pressure of equilibration is 31% of that at the core-mantle boundary. Equilibration in the embryos is assumed to take place at 9 GPa, 2700 K, and $\Delta JW = -2.62$.

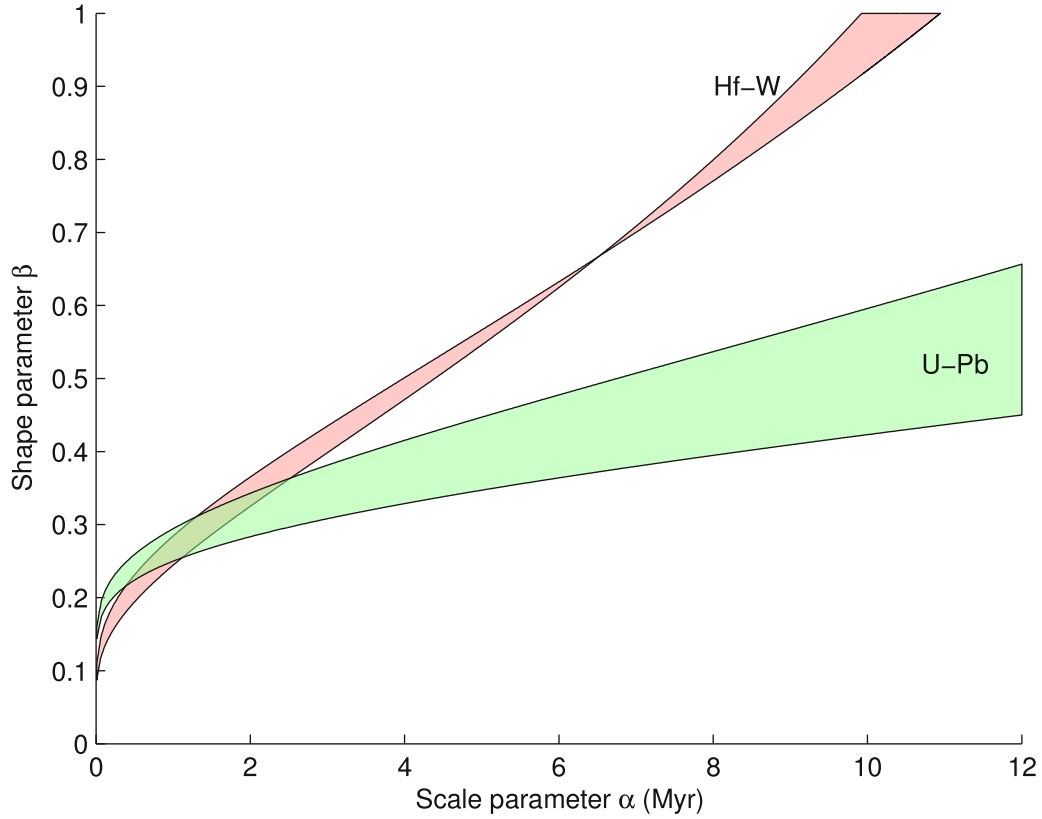


Figure 2: Values of the Weibull time scale parameter α and shape parameter β compatible with the observed isotope systematics. Constant partitioning and full equilibration ($k = 1$) is assumed. For Hf-W the uncertainty due to uncertainty in D_W is shown ($D_W = 21 - 44$). For U-Pb, D_{Pb} is assumed constant, $D_{Pb} = 13$, but the uncertainty due to unknown bulk lead isotopic composition is shown. When $\beta = 1$, the exponential accretion model is recovered, with scale parameters $\alpha^{\text{Hf-W}} = 9.9 - 10.9$ Myr and $\alpha^{\text{U-Pb}} = 21.5 - 50.1$ Myr. There is a region of overlap between Hf-W and U-Pb around $\alpha = 0.4 - 2.5$ Myr, $\beta = 0.22 - 0.36$.

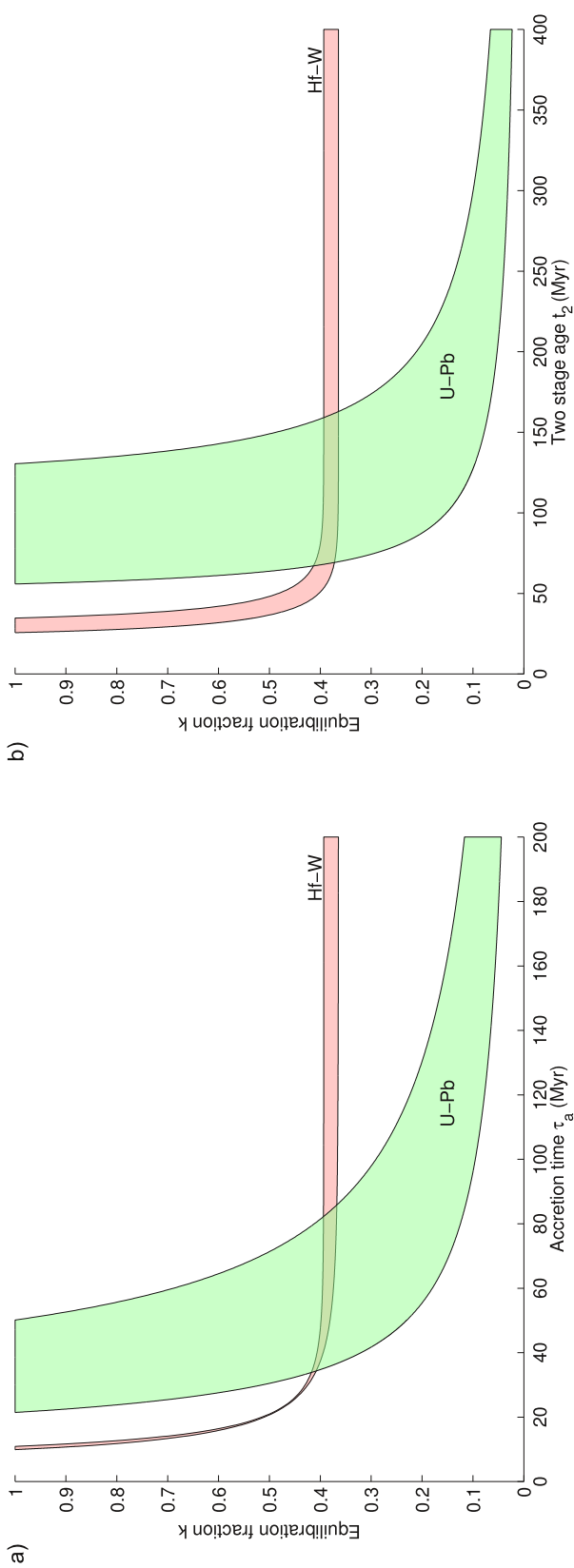


Figure 3: Disequilibrium models with a) exponential accretion and b) step function accretion (two stage model). a) shows exponential mean accretion age τ_a as a function of equilibration fraction k . Uncertainties are as in Figure 2. For full equilibration ($k = 1$) the model age ranges are non-overlapping $\tau_{a,\text{eq}}^{\text{Hf-W}} = 9.9 - 10.9$ Myr and $\tau_{a,\text{eq}}^{\text{U-Pb}} = 21.5 - 50.1$ Myr. b) shows two stage age t_2 as a function of equilibration fraction k . For full equilibration ($k = 1$) the model age ranges are non-overlapping $t_{2,\text{eq}}^{\text{Hf-W}} = 25.7 - 34.8$ Myr and $t_{2,\text{eq}}^{\text{U-Pb}} = 55.9 - 130.5$ Myr. In both a) and b) the region of overlap has k near to the asymptotic values for Hf-W (for very slow accretion $k^{\text{Hf-W}} = 0.36 - 0.39$)

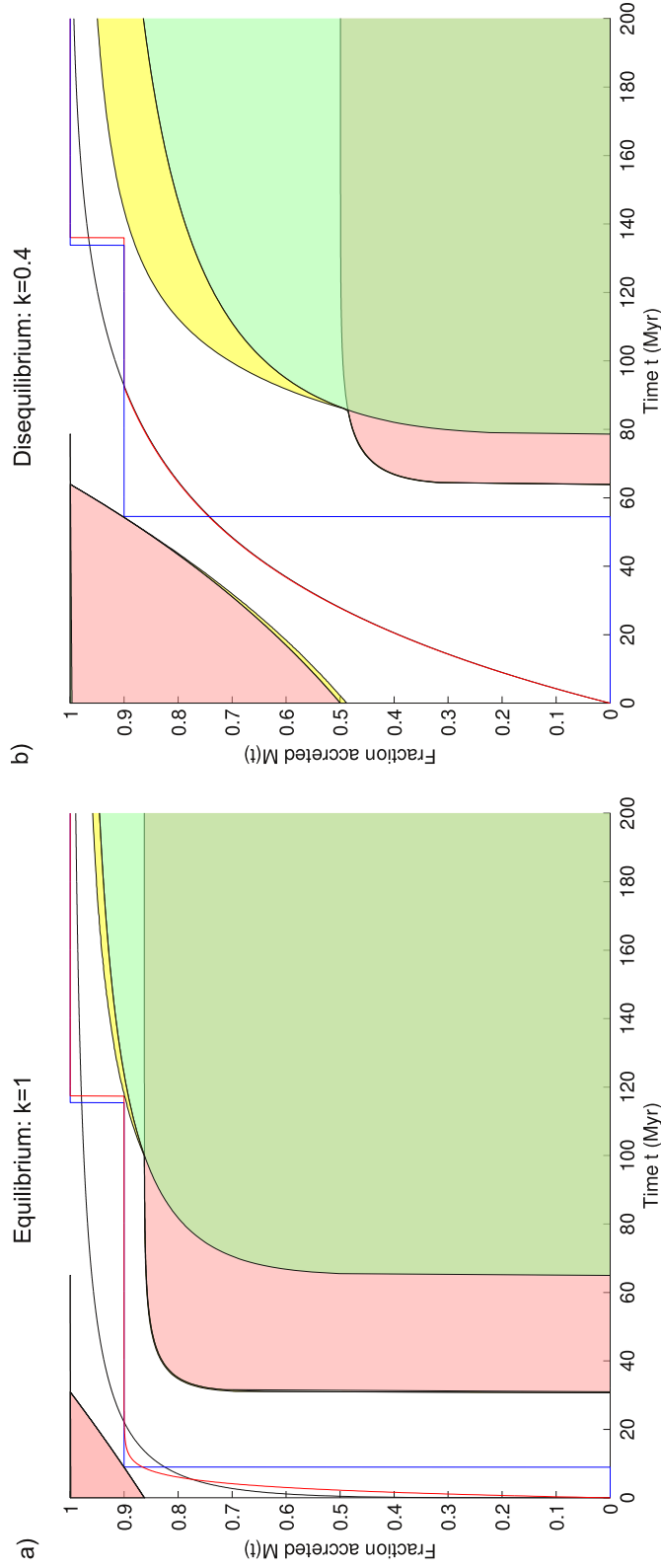


Figure 4: Example accretion curves compatible with both Hf-W and U-Pb isotopic constraints for a) full equilibration ($k = 1$) and b) partial equilibration ($k = 0.4$). Equilibrium two stage ages $t_{2,eq}^{Hf-W} = 31.0$ Myr and $t_{2,eq}^{U-Pb} = 65$ Myr are assumed, with $D_W = 32$ and $D_{Pb} = 13$. These assumed values are demonstrative, not definitive. The shaded regions are forbidden given the Hf-W (pink), U-Pb (green), and combined (yellow) constraints. In a), three example curves are shown: Weibull (black), and two scenarios culminating in a giant impact at around 120 Myr (red/blue)^{2,3}. In b), an exponential model is shown (black) and two scenarios having a giant impact at around 130 Myr (red/blue).

Supplementary Methods

A Model governing equations

The model used throughout this work is a simple box model, a diagram of which can be seen in Supplementary Figure 1, and a summary of notation in Supplementary Table 6. There are two main stages: First the planetary embryos form, and differentiate into a metal core and a silicate mantle. It is assumed that the metal is in chemical equilibrium with the silicate as the embryo differentiates. The second stage comprises the accretion of the Earth from the planetary embryos. The mantle of the planetary embryos directly joins the mantle of the accreting Earth. The core of the planetary embryos takes two different routes to the core of the accreting Earth: A mass fraction k of the incoming core material equilibrates with the Earth’s silicate mantle as it travels to the Earth’s core, whereas a mass fraction $1 - k$ is added directly to the Earth’s core without any equilibration.

A.1 Stable species

Consider first the case of stable species, such as a stable isotope or a trace element. The concentrations of a stable species in the mantle and core of the embryo are given by the usual equilibrium partitioning equations, namely

$$Fc_{ce} + (1 - F)c_{me} = c_b, \quad \frac{c_{ce}}{c_{me}} = D_c \quad (\text{A.1})$$

or

$$c_{me} = \frac{c_b}{FD_c + (1 - F)}, \quad c_{ce} = \frac{D_c c_b}{FD_c + (1 - F)}, \quad (\text{A.2})$$

where c_{me} refers to the concentration in the mantle of the embryo, c_{ce} to the concentration in the core of the embryo, and c_b to the bulk concentration. F represents the mass fraction of metal, which will be assumed to be the same as the Earth’s current core mass fraction, $F = 0.323$. D_c is the metal/silicate partition coefficient for the element in question. In general D_c is a function of the temperature, pressure, and oxygen fugacity conditions under which the metal/silicate equilibration takes place. As a simplifying assumption it will be assumed that all embryo material formed at the same temperature, pressure and oxygen fugacity conditions and thus D_c takes a single value for all embryo material.

The Earth accreted over a period of time, which will be represented by a function $M(t)$ which determines the fraction of the Earth that has accreted at time t , where $t = 0$ represents the beginning of accretion. Thus $M(0) = 0$, and $M(t) = 1$ when accretion has ceased. The entire mass of each embryo is assumed to join the mass of the Earth: we do not model “hit-and-run” collisions^{31,32}, where only part of the embryo material joins the Earth.

Conservation of mass in the accreting Earth can be described by the following equations for the Earth’s mantle and core reservoirs

$$\frac{d}{dt} ((1 - F)M c_m) = [(1 - F) c_{me} + kF (c_{ce} - D_c c_m)] \frac{dM}{dt}, \quad (\text{A.3})$$

$$\frac{d}{dt} (FM c_c) = [kFD_c c_m + (1 - k)F c_{ce}] \frac{dM}{dt}, \quad (\text{A.4})$$

where c_m is the concentration of the chemical species in the Earth's mantle, and c_c is the concentration in the Earth's core. A mass fraction F of the Earth is core, and $1 - F$ is mantle. Thus the quantities $(1 - F)Mc_m$ and FMc_c represent the relative number of moles of the chemical species in the two reservoirs. The two terms on the right hand side of (A.4) represent the two paths that metal from the embryos takes to the Earth's core: $(1 - k)Fc_{ce}$ represents the mass fraction $1 - k$ which travels directly to the core without reequilibration and thus records the embryo concentration, whereas $kFD_c c_m$ represents the mass fraction k which equilibrates with the mantle and thus has a composition in equilibrium with the Earth's mantle. The first term on the right hand side of (A.3), $(1 - F)c_{me}$, represents the mantle embryo material that is added directly to the Earth's mantle, whereas $kF(c_{ce} - D_c c_m)$ represents the change in the Earth's mantle composition due to reequilibration with some of the incoming embryo core material. In general the partition coefficient D_c will be a function of time, since the pressure, temperature, and oxygen fugacity conditions under which metal-silicate equilibration occurred is expected to have changed as the Earth accreted. Note that the bulk concentration of the two reservoirs combined, $Fc_c + (1 - F)c_m = c_b$ remains constant during the accretion, as can be seen by adding (A.3) and (A.4).

(A.3) and (A.4) can be rewritten as evolution equations for the concentrations c_m and c_c ,

$$\frac{dc_m}{dt} = \left[c_{me} + \frac{kF}{1 - F}c_{ce} - \left(1 + \frac{kD_c F}{1 - F} \right) c_m \right] \frac{1}{M} \frac{dM}{dt}, \quad (\text{A.5})$$

$$\frac{dc_c}{dt} = [kD_c c_m + (1 - k)c_{ce} - c_c] \frac{1}{M} \frac{dM}{dt}. \quad (\text{A.6})$$

There is a singularity in the above equation at $t = 0$ as a result of the initial zero mass fraction accreted, $M(0) = 0$. This singularity is removed by imposing the initial conditions $c_m = c_{m0}$ and $c_c = c_{c0}$ where

$$c_{m0} = \frac{c_{me} + kFc_{ce}/(1 - F)}{1 + kFD_c(0)/(1 - F)}, \quad (\text{A.7})$$

$$c_{c0} = \frac{kD_c(0)c_{me} + ((1 - k + kD_c(0)F)/(1 - F))c_{ce}}{1 + kFD_c(0)/(1 - F)}, \quad (\text{A.8})$$

where $D_c(0)$ is the metal/silicate partition coefficient at time 0. The terms in square brackets in (A.5) and (A.6) are then initially zero and the singularity is removed. Starting from these initial conditions, (A.5) and (A.6) may be integrated to obtain the concentrations in the Earth's mantle and core.

A.2 Parent isotope

Suppose a parent isotope p decays to a daughter isotope d with some decay constant λ . For simplicity, we will assume the embryos form at time 0 in the model. The initial concentrations of the parent isotope p in the embryos are given by equilibrium partitioning,

$$p_{me0} = \frac{p_{b0}}{FD_p + (1 - F)}, \quad p_{ce0} = \frac{D_p p_{b0}}{FD_p + (1 - F)}, \quad (\text{A.9})$$

where p_{b0} is the initial bulk concentration. The subsequent evolution in time is given by the usual radioactive decay law

$$p_{me} = p_{me0}e^{-\lambda t}, \quad p_{ce} = p_{ce0}e^{-\lambda t}, \quad p_b = p_{b0}e^{-\lambda t}. \quad (\text{A.10})$$

The concentration of the parent isotope in the Earth’s mantle satisfies

$$\frac{dp_m}{dt} = \left[p_{me} + \frac{kF}{1-F} p_{ce} - \left(1 + \frac{kD_p F}{1-F} \right) p_m \right] \frac{1}{M} \frac{dM}{dt} - \lambda p_m, \quad (\text{A.11})$$

with initial condition

$$p_{m0} = \frac{(1-F)p_{me0} + kFp_{ce0}}{1-F + kFD_p(0)}. \quad (\text{A.12})$$

Similar equations can be written for the Earth’s core.

A.3 Daughter isotope

The initial concentrations of the daughter isotope in the embryo are given by equilibrium partitioning as

$$d_{me0} = \frac{d_{b0}}{FD_d + (1-F)}, \quad d_{ce0} = \frac{D_d d_{b0}}{FD_d + (1-F)}, \quad (\text{A.13})$$

with subsequent evolution due to radioactive decay given by

$$d_{me} = d_{me0} + p_{me0}(1 - e^{-\lambda t}), \quad (\text{A.14})$$

$$d_{ce} = d_{ce0} + p_{ce0}(1 - e^{-\lambda t}), \quad (\text{A.15})$$

$$d_b = d_{b0} + p_{b0}(1 - e^{-\lambda t}). \quad (\text{A.16})$$

The concentration of the daughter isotope in the Earth’s mantle satisfies

$$\frac{dd_m}{dt} = \left[d_{me} + \frac{kF}{1-F} d_{ce} - \left(1 + \frac{kD_d F}{1-F} \right) d_m \right] \frac{1}{M} \frac{dM}{dt} + \lambda p_m, \quad (\text{A.17})$$

with initial condition

$$d_{m0} = \frac{(1-F)d_{me0} + kFd_{ce0}}{1-F + kFD_d(0)}. \quad (\text{A.18})$$

B Analytical solutions for constant partition coefficients

When the partition coefficients vary in time due to changing temperature, pressure, and oxygen fugacity conditions, the differential equations must be solved numerically. However, it is useful to examine the case of constant partition coefficients, where some analytical solutions are possible. Constant partitioning is assumed in Figures 2, 3, and 4. For the case of full equilibration ($k = 1$), the analytical solutions have been reviewed in detail by Jacobsen¹. Here we generalise these solutions to the case of partial equilibration for some constant k , $0 < k < 1$.

B.1 Stable species

We will assume the same constant partition coefficient for both metal/silicate partitioning in the embryos and on Earth. It is convenient to introduce a new variable $R_c = D_c F / (1 - F)$. The embryo concentration in (A.2) can then be rewritten as

$$c_{me} = \frac{1}{1 + R_c} \cdot \frac{c_b}{1 - F}, \quad c_{ce} = \frac{R_c}{1 + R_c} \cdot \frac{c_b}{F}, \quad (\text{B.1})$$

and the initial Earth's mantle concentration from (A.7) is

$$c_{m0} = \frac{1}{1 + kR_c} \left(c_{me} + \frac{kF}{1 - F} c_{ce} \right) = \frac{1}{1 + R_c} \cdot \frac{c_b}{1 - F} = c_{me}. \quad (\text{B.2})$$

The mantle evolution equation from (A.5) is

$$\frac{dc_m}{dt} = (1 + kR_c) (c_{m0} - c_m) \frac{1}{M} \frac{dM}{dt} \quad (\text{B.3})$$

with initial condition $c_m = c_{m0}$. The solution of the above is simply that c_m is constant, $c_m = c_{m0}$ for all time. Thus the concentration is the same in the mantle of the embryos as in the mantle of Earth, and remains constant, as one would expect for the assumed constant partitioning behaviour.

B.2 Parent isotope

The concentrations of the parent isotope in the embryo are from (A.9) and (A.10)

$$p_{me} = \frac{1}{1 + R_p} \cdot \frac{p_{b0}}{1 - F} e^{-\lambda t}, \quad p_{ce} = \frac{R_p}{1 + R_p} \cdot \frac{p_{b0}}{F} e^{-\lambda t}, \quad (\text{B.4})$$

and the initial mantle concentration from (A.12) is

$$p_{m0} = \frac{1}{1 + kR_p} \left(p_{me0} + \frac{kF}{1 - F} p_{ce0} \right) = \frac{1}{1 + R_p} \cdot \frac{p_{b0}}{1 - F} = p_{me0}. \quad (\text{B.5})$$

The mantle evolution from (A.11) is

$$\frac{dp_m}{dt} = (1 + kR_p) \left(p_{m0} e^{-\lambda t} - p_m \right) \frac{1}{M} \frac{dM}{dt} - \lambda p_m \quad (\text{B.6})$$

with initial condition $p_m = p_{m0}$. The solution of the above is simply $p_m = p_{m0} e^{-\lambda t}$.

B.3 Daughter isotope

The concentrations of the daughter isotope in the embryo are from (A.13), (A.14), and (A.15)

$$d_{me} = \frac{1}{1 + R_d} \cdot \frac{d_{b0}}{1 - F} + \frac{1}{1 + R_p} \cdot \frac{p_{b0}}{1 - F} \left(1 - e^{-\lambda t} \right), \quad (\text{B.7})$$

$$d_{ce} = \frac{R_d}{1 + R_d} \cdot \frac{d_{b0}}{F} + \frac{R_p}{1 + R_p} \cdot \frac{p_{b0}}{F} \left(1 - e^{-\lambda t} \right). \quad (\text{B.8})$$

Now, noting that

$$\begin{aligned} d_{me} + \frac{kF}{1 - F} d_{ce} &= \frac{1 + kR_d}{1 + R_d} \frac{d_{b0}}{1 - F} + \frac{1 + kR_p}{1 + R_p} \frac{p_{b0}}{1 - F} \left(1 - e^{-\lambda t} \right) \\ &= (1 + kR_d) d_{m0} + (1 + kR_p) p_{m0} \left(1 - e^{-\lambda t} \right), \end{aligned} \quad (\text{B.9})$$

the evolution of the daughter isotope in the mantle (A.17) may be written as

$$\frac{dd_m}{dt} = \left[(1 + kR_d)(d_{m0} - d_m) + (1 + kR_p)p_{m0} \left(1 - e^{-\lambda t} \right) \right] \frac{1}{M} \frac{dM}{dt} + p_{m0}\lambda e^{-\lambda t} \quad (\text{B.10})$$

with initial condition $d_m = d_{m0}$. The solution to the above can be expressed in integral form as

$$d_m = d_{m0} + p_{m0} \frac{1 + kR_p}{1 + kR_d} \left(1 - e^{-\lambda t} \right) + \frac{k(R_d - R_p)}{1 + kR_d} p_{m0} \int_0^t \left(\frac{M(s)}{M(t)} \right)^{1+kR_d} \lambda e^{-\lambda s} ds, \quad (\text{B.11})$$

which in turn can be rewritten as

$$d_m = d_{m0} + p_{m0} \frac{1 + R_p}{1 + R_d} \left(1 - e^{-\lambda t} \right) + \frac{R_d - R_p}{1 + R_d} p_{m0} \int_0^t \left[\frac{1 - k}{1 + kR_d} + \frac{k(1 + R_d)}{1 + kR_d} \left(\frac{M(s)}{M(t)} \right)^{1+kR_d} \right] \lambda e^{-\lambda s} ds. \quad (\text{B.12})$$

A convenient way of rewriting the integral in the above expression is in terms of an age distribution (see section E for further discussion of age distributions). Let T_d be a random variable with cumulative distribution function (CDF)

$$\mathbb{P}(T_d \leq s) = \frac{1 - k}{1 + kR_d} + \frac{k(1 + R_d)}{1 + kR_d} \left(\frac{M(s)}{M(t)} \right)^{1+kR_d}, \quad 0 < s < t \quad (\text{B.13})$$

with $\mathbb{P}(T_d \leq s) = 0$ for $s < 0$ and $\mathbb{P}(T_d \leq s) = 1$ for $s > t$. The corresponding probability density function (PDF) is

$$\rho(s) = \frac{1 - k}{1 + kR_d} \delta(s) + k(1 + R_d) \left(\frac{M(s)}{M(t)} \right)^{kR_d} \frac{\dot{M}(s)}{M(t)}, \quad (\text{B.14})$$

where $\delta(s)$ is the Dirac delta function. $\rho(s) = 0$ for $s < 0$ and $s > t$. The integral expression on the right hand side of (B.12) is thus

$$\int_0^t \mathbb{P}(T_d \leq s) \lambda e^{-\lambda s} ds = \int_{0-}^t \rho(s) \left(e^{-\lambda t} - e^{-\lambda s} \right) ds = \mathbb{E} \left(e^{-\lambda t} - e^{-\lambda T_d} \right) \quad (\text{B.15})$$

where \mathbb{E} denotes expectation. Thus we can write (B.12) more compactly as

$$d_m = d_{m0} + p_{m0} \frac{1 + R_p}{1 + R_d} \left(1 - e^{-\lambda t} \right) + \frac{R_p - R_d}{1 + R_d} p_{m0} \mathbb{E} \left(e^{-\lambda T_d} - e^{-\lambda t} \right). \quad (\text{B.16})$$

Consider now a stable reference isotope d' , which is of the same element as d but neither decays nor is a decay product. Thus $d'_m = d'_{m0}$. Since

$$\left(\frac{d}{d'} \right)_{m0} = \left(\frac{d}{d'} \right)_{b0}, \quad \left(\frac{p}{d'} \right)_{m0} = \frac{1 + R_d}{1 + R_p} \left(\frac{p}{d'} \right)_{b0}, \quad (\text{B.17})$$

on dividing (B.16) by d'_m we have

$$\left(\frac{d}{d'}\right)_m = \left(\frac{d}{d'}\right)_{b0} + \left(\frac{p}{d'}\right)_{b0} (1 - e^{-\lambda t}) + \left[\left(\frac{p}{d'}\right)_{m0} - \left(\frac{p}{d'}\right)_{b0}\right] \mathbb{E}(e^{-\lambda T_d} - e^{-\lambda t}). \quad (\text{B.18})$$

Since the bulk evolution satisfies

$$\left(\frac{d}{d'}\right)_b = \left(\frac{d}{d'}\right)_{b0} + \left(\frac{p}{d'}\right)_{b0} (1 - e^{-\lambda t}), \quad (\text{B.19})$$

(B.18) can be rewritten as

$$\frac{(d/d')_m - (d/d')_b}{(p/d')_{m0} - (p/d')_{b0}} = \mathbb{E}(e^{-\lambda T_d} - e^{-\lambda t}) \quad (\text{B.20})$$

or

$$\frac{(d/d')_m - (d/d')_b}{(p/d')_m - (p/d')_b} = \mathbb{E}(e^{\lambda(t-T_d)} - 1). \quad (\text{B.21})$$

(B.20) is the more useful form for extinct isotope systems such as Hf-W, since the present day concentrations of the parent isotope are negligible. Given a reference isotope p' for the parent, (B.20) may be rewritten as

$$\frac{(d/d')_m - (d/d')_b}{(p/p')_{b0} [(p'/d')_m - (p'/d')_b]} = \mathbb{E}(e^{-\lambda T_d} - e^{-\lambda t}), \quad (\text{B.22})$$

which is similar to the usual form in which Hf-W model ages are expressed. For extinct systems like Hf-W, $e^{-\lambda t}$ is essentially zero at the present day. (B.20), (B.21), and (B.22) are very similar to the usual expressions for a two stage model age. Indeed, the aim of introducing the random variable T_d is to make this similarity clear. The usual expressions for a two stage age with full equilibration drop the expectations and have T_d replaced by the equilibrium two stage age $t_{2,\text{eq}}$. Thus

$$\mathbb{E}(e^{-\lambda T_d}) = e^{-\lambda t_{2,\text{eq}}}. \quad (\text{B.23})$$

C Relationships between model ages

(B.23) is the fundamental equation for comparing different model ages. The equilibrium two stage age on the right hand side can be estimated from the current mantle and bulk compositions. The left hand side depends on the accretion rate through $M(t)$, the amount of equilibration through k , and the enrichment of the daughter isotope in the metal during partitioning through R_d . Different models assume different forms for $M(t)$, and different amounts of equilibration k . To compare the different models, we must study the behaviour of $\mathbb{E}(e^{-\lambda T_d})$. Different models should give equal values for this quantity in order to fit the same observations. Note that for long lived isotope systems such as U-Pb, $\mathbb{E}(e^{-\lambda T_d}) \approx 1 - \lambda \mathbb{E}(T_d)$, and thus for such systems $\mathbb{E}(T_d)$ takes the same value between different models. It is convenient to introduce a new random variable S_d with cumulative distribution function

$$\mathbb{P}(S_d \leq s) = (M(s))^{1+kR_d}, \quad s > 0 \quad (\text{C.1})$$

which is related to T_d by (B.13)

$$\mathbb{P}(T_d \leq s) = \frac{1-k}{1+kR_d} + \frac{k(1+R_d)}{1+kR_d} \mathbb{P}(S_d \leq s), \quad s > 0. \quad (\text{C.2})$$

In the above it has been assumed that we are considering the present day, where accretion is complete ($M(t) = 1$). It follows that

$$\mathbb{E}(1 - e^{-\lambda T_d}) = \frac{k(1+R_d)}{1+kR_d} \mathbb{E}(1 - e^{-\lambda S_d}), \quad (\text{C.3})$$

$$\mathbb{E}(T_d) = \frac{k(1+R_d)}{1+kR_d} \mathbb{E}(S_d). \quad (\text{C.4})$$

From (C.3) it follows that if we know $\mathbb{E}(e^{-\lambda T_d})$, we know $\mathbb{E}(e^{-\lambda S_d})$. Models that differ only in the form of $M(t)$ must share the same value of $\mathbb{E}(e^{-\lambda S_d})$ in order to be compatible with the same observations. However, models that differ in the degree of equilibration k will have different values of $\mathbb{E}(e^{-\lambda S_d})$, but will still have the same values of $\mathbb{E}(e^{-\lambda T_d})$.

C.1 Two stage ages

The simplest model is a two stage model, where there is no accretion until a certain time, and then all the accretion occurs at once. The function $M(t)$ is then a step function,

$$M(t) = \begin{cases} 0, & 0 < t < t_2, \\ 1, & t > t_2, \end{cases} \quad (\text{C.5})$$

where t_2 is the corresponding two stage age. For the above choice of $M(t)$ we have

$$\mathbb{E}(e^{-\lambda S_d}) = e^{-\lambda t_2}, \quad (\text{C.6})$$

$$\mathbb{E}(S_d) = t_2. \quad (\text{C.7})$$

Thus we can relate the two stage age $t_{2,\text{eq}}$ that occurs with full equilibration ($k = 1$) with a two stage age t_2 that occurs with partial equilibration ($0 < k < 1$) using (B.23), (C.3), and (C.6)

$$1 - e^{-\lambda t_{2,\text{eq}}} = \frac{k(1+R_d)}{1+kR_d} (1 - e^{-\lambda t_2}). \quad (\text{C.8})$$

This relationship is plotted in Figure 3b. It can be approximated for long-lived systems as

$$t_{2,\text{eq}} \approx \frac{k(1+R_d)}{1+kR_d} t_2. \quad (\text{C.9})$$

For general λ , Jensen's inequality on (B.23) combined with (C.4) and (C.7) implies

$$t_{2,\text{eq}} \leq \mathbb{E}(T_d) = \frac{k(1+R_d)}{1+kR_d} t_2 \leq t_2, \quad (\text{C.10})$$

and hence disequilibrium always increases the two stage age. From (C.8), the following inequality holds for k ,

$$\frac{1 - e^{-\lambda t_{2,\text{eq}}}}{1 + R_d e^{-\lambda t_{2,\text{eq}}}} \leq k \leq 1, \quad (\text{C.11})$$

and hence there is a lower bound on the amount of disequilibrium. These inequalities become equalities as $\lambda t_2 \rightarrow \infty$, and $t_2 \rightarrow t_{2,\text{eq}}$ respectively.

C.2 Exponential accretion

One of the simplest continuous models of accretion is to assume an exponential accretion with a mean age τ_a , namely

$$M(t) = 1 - e^{-t/\tau_a}. \quad (\text{C.12})$$

The relevant moments are

$$\mathbb{E}(e^{-\lambda S_d}) = \frac{\Gamma(2 + kR_d)\Gamma(1 + \lambda\tau_a)}{\Gamma(2 + kR_d + \lambda\tau_a)}, \quad (\text{C.13})$$

where $\Gamma(x)$ is the gamma function, and

$$\mathbb{E}(S_d) = \tau_a H_{1+kR_d}, \quad (\text{C.14})$$

where H_x is the x^{th} harmonic number, which can be expressed for general x as $H_x = \gamma + \Psi(1 + x)$, where γ is the Euler-Maschoroni constant, and Ψ is the digamma function.

Comparing the expressions for $\mathbb{E}(e^{-\lambda S_d})$ in (C.6) and (C.13), we see there is the following relationship between the two stage age t_2 and the exponential mean age of accretion τ_a ,

$$e^{-\lambda t_2} = \frac{\Gamma(2 + kR_d)\Gamma(1 + \lambda\tau_a)}{\Gamma(2 + kR_d + \lambda\tau_a)}, \quad (\text{C.15})$$

and this used in plotting Figure 3a. It can be approximated for long lived systems using (C.7) and (C.14) as

$$t_2 \approx \tau_a H_{1+kR_d}. \quad (\text{C.16})$$

For long-lived systems, the two stage age is thus always greater than the exponential mean age of accretion, $t_2 \geq \tau_a$. However, in general, the two stage age can be less than or greater than the mean age of accretion depending on kR_d and λ . Independent of λ , the ages satisfy $t_2 \leq \tau_a H_{1+kR_d}$, by Jensen's inequality on (C.6). Typical values are $R_W \sim 16$ and $R_{\text{Pb}} \sim 7$ which give $H_{1+R_W} \sim 3.4$ and $H_{1+R_{\text{Pb}}} \sim 2.7$. Thus with full equilibration ($k = 1$) the two stage model ages for Hf-W and U-Pb are around 3 times larger than the exponential model ages, i.e. the two stage model ages relate to the point of $\sim 95\%$ accretion in the exponential models ($1 - e^{-3} = 0.95$).

For integer values of kR_d , (C.15) can be expanded as (exploiting the fact that $\Gamma(x) = (x - 1)!$ for integer x)

$$e^{-\lambda t_2} = \prod_{r=1}^{1+kR_d} \left(1 + \frac{\lambda\tau_a}{r}\right)^{-1} \quad (\text{C.17})$$

and rewritten as

$$t_2 = \frac{1}{\lambda} \sum_{r=1}^{1+kR_d} \log \left(1 + \frac{\lambda\tau_a}{r}\right) \quad (\text{C.18})$$

which agrees with the relationship quoted by Jacobsen¹ (his equation (77)) in the case of full equilibration. (C.15) is more general as it encompasses partial equilibration, and holds for non-integer values of the parameters.

C.3 Weibull accretion

A useful two parameter accretion model is

$$M(t) = 1 - e^{-(t/\alpha)^\beta}, \quad (\text{C.19})$$

which is known as the Weibull distribution with time scale parameter α and shape parameter β . The corresponding mean age of accretion is $\alpha\Gamma(1 + 1/\beta)$. The Weibull distribution encompasses both the models described above for appropriate choices of the shape parameter: $\beta = 1$ is the exponential model, and as $\beta \rightarrow \infty$ the step function is recovered. For the Weibull model there are no simple closed form expressions for the moments $\mathbb{E}(e^{-\lambda S_d})$ and $\mathbb{E}(S_d)$, and the integrals need to be evaluated numerically (Figure 2).

Weibull models with $\beta \leq 1$ have their maximum rates of accretion (dM/dt) at time $t = 0$, while Weibull models with $\beta > 1$ have their maximum rates of accretion at later times $t > 0$. To get a match between Hf-W and U-Pb with a Weibull model, $\beta < 1$ is required (Figure 2), but this does not imply that Earth’s accretion was actually at its most rapid at time 0 (the time of CAI formation). Physical models suggest there may have been a very early stage of slow accretion, followed by rapid accretion and finally a very slow and protracted late accretion²⁷. If the duration of the very early stage of slow accretion was significantly shorter than the half life of ¹⁸²Hf then it would have had little influence on the subsequent isotopic evolution. A very early stage of slow accretion could be added to the model without influencing the main result: namely that a stage of rapid early accretion followed by a stage of protracted late accretion is required.

D Bounds on accretion

D.1 Analytical bounds

There are some general bounds that can be placed on the accretion curve $M(t)$ without assuming any particular parametric form. Markov’s inequality applied to $e^{-\lambda S_d}$ is

$$\mathbb{P}(e^{-\lambda S_d} \geq e^{-\lambda t}) \leq \frac{\mathbb{E}(e^{-\lambda S_d})}{e^{-\lambda t}} \quad (\text{D.1})$$

which implies

$$\mathbb{P}(S_d \leq t) \leq e^{\lambda t} \mathbb{E}(e^{-\lambda S_d}) = e^{\lambda(t-t_2)}, \quad (\text{D.2})$$

and thus the following bound can be placed on $M(t)$ using (C.1),

$$M(t) \leq e^{\lambda(t-t_2)/(1+kR_d)}, \quad (\text{D.3})$$

which bounds the early accretion ($t \leq t_2$, Figure 4). Notably, the accretion cannot finish until $t \geq t_2$. This bound is achieved by step function accretion curves of the form

$$M(t) = \begin{cases} 0, & 0 < t < t_c, \\ e^{\lambda(t_c-t_2)/(1+kR_d)}, & t_c < t < \infty, \end{cases} \quad (\text{D.4})$$

for $t_c \leq t_2$.

Applying Markov's inequality to $1 - e^{-\lambda S_d}$ gives

$$\mathbb{P}(1 - e^{-\lambda S_d} \geq 1 - e^{-\lambda t}) \leq \frac{\mathbb{E}(1 - e^{-\lambda S_d})}{1 - e^{-\lambda t}} \quad (\text{D.5})$$

which implies

$$\mathbb{P}(S_d \leq t) \geq \frac{\mathbb{E}(e^{-\lambda S_d}) - e^{-\lambda t}}{1 - e^{-\lambda t}} = \frac{e^{-\lambda t_2} - e^{-\lambda t}}{1 - e^{-\lambda t}}, \quad (\text{D.6})$$

and thus the following bound can be placed on $M(t)$,

$$M(t) \geq \left(\frac{e^{-\lambda t_2} - e^{-\lambda t}}{1 - e^{-\lambda t}} \right)^{1/(1+kR_d)}, \quad (\text{D.7})$$

which bounds the late accretion ($t \geq t_2$, [Figure 4](#)). This bound is achieved by step function accretion curves of the form

$$M(t) = \begin{cases} \left(\frac{e^{-\lambda t_2} - e^{-\lambda t}}{1 - e^{-\lambda t}} \right)^{1/(1+kR_d)}, & 0 < t < t_c, \\ 1, & t > t_c, \end{cases} \quad (\text{D.8})$$

for $t_c \geq t_2$.

Bounds can also be placed on the mean age of accretion. Let T_{acc} be a random variable with CDF $M(t)$. Then, from the inequality,

$$1 - (M(t))^n \leq n(1 - M(t)), \quad n \geq 1 \quad (\text{D.9})$$

it follows that

$$\mathbb{E}(S_d) \leq (1 + kR_d)\mathbb{E}(T_{\text{acc}}), \quad (\text{D.10})$$

where $\mathbb{E}(T_{\text{acc}})$ is the mean age of accretion. Similarly, from the inequality

$$1 - (M(t))^n \geq 1 - M(t), \quad n \geq 1 \quad (\text{D.11})$$

it follows that

$$\mathbb{E}(S_d) \geq \mathbb{E}(T_{\text{acc}}). \quad (\text{D.12})$$

Jensen's inequality implies that

$$\mathbb{E}(e^{-\lambda S_d}) \geq e^{-\lambda \mathbb{E}(S_d)}. \quad (\text{D.13})$$

Since $\mathbb{E}(e^{-\lambda S_d}) = e^{-\lambda t_2}$, it follows that

$$t_2 \leq \mathbb{E}(S_d). \quad (\text{D.14})$$

Thus the mean age of accretion can be bounded by

$$\frac{t_2}{1 + kR_d} \leq \frac{\mathbb{E}(S_d)}{1 + kR_d} \leq \mathbb{E}(T_{\text{acc}}) \leq \mathbb{E}(S_d). \quad (\text{D.15})$$

For long-lived systems $\mathbb{E}(S_d) \approx t_2$, and the two stage age t_2 is then an approximate upper bound on the mean age of accretion.

D.2 Numerical bounds

Bounds on the accretion curve $M(t)$ can also be calculated numerically. Suppose $M(t)$ is discretised as a sequence of steps, with $M(t) = M_i$ for $t_{i-1} < t < t_i$, where $t_1 \leq t_2 \leq \dots \leq t_n$ are the given times of the steps. Bounding $M(t)$ is then a matter of solving a nonlinear optimisation problem: Minimising or maximising M_j for a given j subject to the constraints

$$0 \leq M_1 \leq M_2 \leq \dots \leq M_n \leq 1, \quad (\text{D.16})$$

$$1 - e^{-\lambda t_2} = \sum_{i=1}^n \left(e^{-\lambda t_{i-1}} - e^{-\lambda t_i} \right) \left(1 - M_i^{1+kR_d} \right). \quad (\text{D.17})$$

(D.16) ensures the accretion curve is valid, and (D.17) ensures the isotopic observations are matched. The above problem can be solved using standard optimisation algorithms. The advantage of a numerical solution is that multiple constraints can be included, and thus bounds that include both Hf-W and U-Pb constraints can be calculated (yellow region, Figure 4). A similar method can be used to numerically calculate bounds on the mean age of accretion using the objective function

$$\sum_{i=1}^n (t_i - t_{i-1}) (1 - M_i) \quad (\text{D.18})$$

and the same constraints.

E Interpretation of age distributions

Age distributions were introduced in section B in order to represent various integral expressions in a more compact form. However, it should be noted that these age distributions arise naturally from residence time theory, which treats transitions between reservoirs as a Poisson process^{33,34}. This can be best illustrated for the equilibrium case ($k = 1$). Conservation of mass for a stable species in the mantle reservoir (A.3) can be written as

$$\frac{dn_m}{dt} = c_b \frac{dM}{dt} - \frac{R_c}{M} \frac{dM}{dt} n_m \quad (\text{E.1})$$

where $n_m = (1 - F)M c_m$, the relative number of moles in the mantle reservoir. In terms of residence time theory, we can identify

$$\mathbb{P}(\text{m} \rightarrow \text{c}) = \frac{R_c}{M} \frac{dM}{dt} \delta t \quad (\text{E.2})$$

as the probability that an atom in Earth's mantle reservoir will transition to Earth's core reservoir in a time interval δt . This probability varies in time, and is zero once accretion has ceased. By integration, we find that the probability that an atom which was in the Earth's mantle reservoir at time t is still in the Earth's mantle by the end of accretion is

$$\mathbb{P}(\text{atom in m at present} | \text{atom in m at time } t) = (M(t))^{R_c}. \quad (\text{E.3})$$

At time t , the number of atoms which arrive in Earth's mantle reservoir in a time interval δt is

$$c_b \frac{dM}{dt} \delta t \quad (\text{E.4})$$

of which

$$c_b \frac{dM}{dt} (M(t))^{R_c} \delta t \quad (\text{E.5})$$

will remain in Earth’s mantle at the end of accretion. Hence

$$\rho(t) = (1 + R_c) \frac{dM}{dt} (M(t))^{R_c} \quad (\text{E.6})$$

is a probability density function which gives the probability that an atom in Earth’s mantle at present arrived there at time t . The corresponding cumulative distribution function is

$$\mathbb{P}(T_c \leq t) = (M(t))^{1+R_c}. \quad (\text{E.7})$$

Alternatively, $t - T_c$ is a random variable which gives the amount of time an atom has spent in the mantle reservoir, i.e. it is a random variable giving the distribution of residence times in the mantle reservoir. It is this residence time information for the daughter element which gets encoded in the isotopic observations.

Interpreting the age distributions in the general non-equilibrium ($k < 1$) case (i.e. (B.13)) is less straightforward, but essentially represents a mixture of unequilibrated zero age material and equilibrated material with a distribution of ages similar to the above.

F Isotopic parameters and calculated model ages

The Hf-W isotopic system consists of parent $p = {}^{182}\text{Hf}$, daughter $d = {}^{182}\text{W}$, and reference isotopes $p' = {}^{180}\text{Hf}$ and $d' = {}^{184}\text{W}$. Numerical values for the parameters describing the Hf-W isotopic system are given in Supplementary Table 1. These values yield an equilibrium two stage age $t_{2,\text{eq}} = 31.0 \pm 4.4$ Myr and equilibrium exponential accretion time $\tau_{a,\text{eq}} = 10.6 \pm 0.5$ Myr, assuming constant partition coefficients. The predominant uncertainty is in the Hf/W value of the mantle relative to that of the bulk, which leads to an uncertainty in the assumed constant partition coefficient, $D_W = 32.5 \pm 11.0$. Hf is thought not to enter the core, and thus $D_{\text{Hf}} = 0$.

The U-Pb isotopic system consists of two parent isotopes $p = {}^{238}\text{U}, {}^{235}\text{U}$, with respective daughter isotopes $d = {}^{206}\text{Pb}, {}^{207}\text{Pb}$ and common reference isotope $d' = {}^{204}\text{Pb}$. Numerical values for the parameters describing the U-Pb isotopic system are given in Supplementary Table 2. The mantle $({}^{206}\text{Pb}/{}^{204}\text{Pb})_{\text{m}}$ and $({}^{207}\text{Pb}/{}^{204}\text{Pb})_{\text{m}}$ isotopic ratios are not well constrained, as U/Pb fractionation has been ongoing in the Earth due to crust/mantle differentiation. Different literature estimates for the bulk silicate Earth lead isotopic composition are given in Supplementary Table 3 (after Halliday¹⁵). As was pointed out by Kamber and Kramers²⁰, using some of the estimates in Supplementary Table 3 to calculate a two stage age is circular, as some of the authors assumed a particular two stage age from the outset when constructing their estimates^{35,36}. However, not all of the estimates are circular, and they still provide a reasonable guide to the uncertainties involved³⁷.

Unfortunately, the $({}^{238}\text{U}/{}^{204}\text{Pb})_{\text{b}} \equiv \mu_{\text{b}}$ isotopic ratio of the bulk Earth is not well constrained either, due to the volatility of lead. Estimates of μ_{b} range from 0.7¹⁷-1.4³⁸. The mantle value is better constrained, with $\mu_{\text{m}} = 7 - 9$ being a typical estimate¹⁷. These estimates imply a range for the lead partition coefficient, $D_{\text{Pb}} = 8 - 25$. Wood et al.²⁸ have suggested a value of $D_{\text{Pb}} \sim 13$ based on experimental partitioning studies, and this is the

value adopted here (and used in the calculations for Figures 2, 3, and 4). It is assumed that U does not enter the core to any great extent, so $D_U = 0$.

Given the partition coefficient estimate $D_{\text{Pb}} = 13$, the estimates of $(^{206}\text{Pb}/^{204}\text{Pb})_{\text{m}}$ and $(^{207}\text{Pb}/^{204}\text{Pb})_{\text{m}}$ can be combined with the parameters in Supplementary Table 2 to infer the model ages $t_{2,\text{eq}}$ and $\tau_{a,\text{eq}}$, along with μ_{b} and μ_{m} . This is done in Supplementary Table 3. The values estimated for μ_{b} and μ_{m} are broadly consistent with the estimates above. There is a wide range in the estimated model ages, $t_{2,\text{eq}} = 55.9 - 130.5$ Myr and $\tau_{a,\text{eq}} = 21.6 - 51.0$ Myr (using all but the two most extreme estimates from Supplementary Table 3), but nevertheless the ages are notably different from those obtained for Hf-W. The bounds of Figure 4 are calculated using a U-Pb two stage age of $t_{2,\text{eq}} = 65.0$ Myr, but it should be noted that this is simply chosen as a reasonably representative value, to illustrate the kind of constraints that Pb isotopes provide, and is not a definitive value.

G Parametrisation of metal/silicate partition coefficients

Metal/silicate partition coefficients depend on temperature, pressure, and oxygen fugacity conditions. Here we have used the metal/silicate partition coefficient parametrisation of Wade and Wood^{6,7,28,29}, which is outlined below. For a fuller description the reader is referred to the original papers.

Oxygen fugacity is defined relative the iron-wüstite (IW) buffer as

$$\Delta IW = 2 \log_{10} \left(\gamma_{\text{FeO}}^{\text{sil}} / \gamma_{\text{Fe}}^{\text{met}} \right) + 2 \log_{10} \left(x_{\text{FeO}}^{\text{sil}} / x_{\text{Fe}}^{\text{met}} \right), \quad (\text{G.1})$$

where ΔIW is the oxygen fugacity relative to the IW buffer in \log_{10} units. $\gamma_{\text{Fe}}^{\text{met}}$ and $\gamma_{\text{FeO}}^{\text{sil}}$ are the activity coefficients of Fe and FeO in the metal and silicate respectively, and $x_{\text{Fe}}^{\text{met}}$ and $x_{\text{FeO}}^{\text{sil}}$ are the corresponding molar concentrations. The activity coefficients of elements in the metal phase are assumed to depend on temperature as

$$\gamma_{\text{M}}^{\text{met}}(T) = \left(\gamma_{\text{M}}^{\text{met}}(T_0) \right)^{T_0/T} \quad (\text{G.2})$$

where $\gamma_{\text{M}}^{\text{met}}(T_0)$ is the activity at a reference temperature of $T_0 = 1873$ K. Formally, the activity coefficients should also depend on pressure and composition, but for simplicity this dependence is neglected here, and $\gamma_{\text{M}}^{\text{met}}(T_0)$ is assumed constant. The activities $\gamma_{\text{M}}^{\text{met}}(T_0)$ at the reference temperature were calculated by an interaction parameter approach³⁹, with an assumed metal composition, and are given in Supplementary Table 4. The activity of FeO in the silicate is assumed to be independent of temperature, with $\gamma_{\text{FeO}}^{\text{sil}} = 3$. Different choices for $\gamma_{\text{FeO}}^{\text{sil}}$ affect the absolute values of the oxygen fugacity, but the relative results will remain the same.

Using (G.1) and (G.2), the molar Fe metal/silicate partition coefficient can be written as a function of oxygen fugacity as

$$\log_{10} D_{\text{Fe}}^* \equiv \log_{10} \left(x_{\text{Fe}}^{\text{met}} / x_{\text{FeO}}^{\text{sil}} \right) = -\frac{1}{2} \Delta IW - \frac{T_0}{T} \log_{10} \gamma_{\text{Fe}}^{\text{met}}(T_0) + \log_{10} \gamma_{\text{FeO}}^{\text{sil}}. \quad (\text{G.3})$$

The partitioning of the other elements is parametrised relative to the iron partitioning as

$$\log_{10} D_{\text{M}}^* = a + b \frac{1}{T} + c \frac{P}{T} + dN + \frac{v}{2} \log_{10} D_{\text{Fe}}^* + \frac{T_0}{T} \left(\frac{v}{2} \log_{10} \gamma_{\text{Fe}}^{\text{met}}(T_0) - \log_{10} \gamma_{\text{M}}^{\text{met}}(T_0) \right) \quad (\text{G.4})$$

which can be rewritten as

$$\log_{10} D_M^* = a + b \frac{1}{T} + c \frac{P}{T} + dN - \frac{v}{4} \Delta IW - \frac{T_0}{T} \log_{10} \gamma_M^{\text{met}}(T_0) + \frac{v}{2} \log_{10} \gamma_{\text{FeO}}^{\text{sil}}. \quad (\text{G.5})$$

a , b , c , and d are coefficients obtained by regression of experimental data, given in Supplementary Table 4. v is the assumed valence (which for W is also found by regression as it has mixed valence states³⁰). T is the temperature (in K), P is the pressure (in GPa), and N is the molar ratio of non-bridging oxygens to tetrahedral cations in the silicate melt (assumed constant at 2.7). (G.3), (G.4), and (G.5) parametrise the molar partition coefficients D_M^* , but what is of usual interest is the partition coefficients by mass, namely

$$D_M = c_M^{\text{met}} / c_M^{\text{sil}}, \quad (\text{G.6})$$

where c refers to concentration by mass. However, to a good approximation it is found that $D_M \approx D_M^*$, and we will use molar and mass partition coefficients interchangeably.

Target values for the partition coefficients can be obtained from estimates of the present day mantle c_m and core c_c abundances, namely

$$D^{\text{obs}} = c_c / c_m. \quad (\text{G.7})$$

Estimated values are given in Supplementary Table 5. Note that these target values should be compared to integrated values of the true partition coefficients over the different pressure, temperature, and oxygen fugacity conditions that have been experienced during metal silicate-equilibration over the course of the Earth's accretion.

H Pressure, temperature, and oxygen fugacity evolution

To complete the model, the pressure, temperature and oxygen fugacity conditions under which metal silicate equilibration takes place must be specified. The approach taken here is based on that of Wade and Wood⁶, where it postulated that the point of last metal-silicate equilibration takes place at the base of a deep magma ocean. This final metal-silicate equilibration is assumed to take place on the peridotite liquidus, which we approximate by

$$T = 1973 + 28.57P, \quad (\text{H.1})$$

where T is in K and P is in GPa. The pressure of equilibration is assumed to evolve as

$$P(t) = P_0(M(t))^{2/3}, \quad (\text{H.2})$$

for some constant P_0 to be determined. The assumed scaling of $(M(t))^{2/3}$ reflects the increase in pressure with planet size, which scales as the square of the planet radius. The pressure P_0 can be associated with an average depth of magma ocean equilibration through $h_0/h_{\text{cmb}} = P_0/P_{\text{cmb}}$, where P_{cmb} and h_{cmb} are the present day core-mantle boundary pressure and depth ($P_{\text{cmb}} = 135$ GPa, $h_{\text{cmb}} = 2886$ km).

Finally, the oxygen fugacity state is allowed to evolve as the planet accretes. We assume the following simple form, based on that of Corgne et al⁷,

$$\Delta IW = \begin{cases} \Delta IW_1, & 0 < M(t) < 0.1, \\ \Delta IW_1 + (\Delta IW_2 - \Delta IW_1) \frac{M(t) - 0.1}{0.9}, & 0.1 < M(t) < 1, \end{cases} \quad (\text{H.3})$$

for initial oxygen fugacity ΔIW_1 and final oxygen fugacity ΔIW_2 . The oxygen fugacity remains constant for the first 10% of the accretion, and then increases linearly for the remainder of the accretion.

I Trace element inversion

Values of the parameters P_0 , ΔIW_1 and ΔIW_2 that best fit the observations are obtained by inversion, using a penalty function approach (Figure 1). Having these three free parameters seems to be the minimum needed to get a good match to the observations. The chosen penalty function to minimise is

$$g(P_0, \Delta IW_1, \Delta IW_2) = \sum_{i=1}^n \left(\frac{\log_{10} D_i^{\text{model}} - \log_{10} D_i^{\text{obs}}}{\sigma_i} \right)^2 \quad (\text{I.1})$$

where D_i^{model} is the overall partition coefficient that is obtained from integrating the model, namely $D^{\text{model}} = c_c/c_m$. $i = 1, 2, \dots, n$ refer to the n trace elements that are used for inversion. Only a subset of the available trace elements are used in the inversion (Fe, Ni, Co, V, W, Si, Nb, Ta), since these elements are the most refractory and their bulk Earth abundances are thus best constrained. The uncertainties σ_i^2 arise from two sources: uncertainties in the experimentally derived partition coefficients D_i^* , which lead to uncertainties in D_i^{model} on integrating the model (shown as red error bars in Figure 1), and uncertainties in the present day elemental abundances, which lead to uncertainties in D_i^{obs} (shown as blue error bars in Figure 1). The total uncertainty is given by

$$\sigma_i^2 = \sigma_{\log_{10} D_i^{\text{model}}}^2 + \sigma_{\log_{10} D_i^{\text{obs}}}^2, \quad (\text{I.2})$$

which is used to weight the different terms in (I.1). The lower the uncertainty, the greater weight that is placed on that term in the penalty function. Thus certain elements influence the penalty function more strongly than others, as some elements have better constrained abundances and partitioning behaviours. The 1σ uncertainties on $\log_{10} D^{\text{obs}}$ are given in Supplementary Table 5, and the 1σ uncertainties on the experimental regression coefficients for D^* are given in Supplementary Table 4. The error propagation to determine the uncertainty on D^{model} proceeds under the assumption of independent errors, namely

$$\sigma_{\log_{10} D^*}^2 = \sigma_a^2 + \sigma_b^2 \frac{1}{T^2} + \sigma_c^2 \frac{P^2}{T^2} + \sigma_d^2 N^2 + \frac{\sigma_v^2}{16} \Delta IW^2. \quad (\text{I.3})$$

Different studies report errors in different ways, which makes comparing errors between studies difficult. For the studies considered here, the most noticeable difference is that Cottrell et al.³⁰ report errors on all regression coefficients (v, a, b, c, d) whereas the other studies^{6,7,28,29} only report errors on the coefficients c and d (and also b for the case of Cr in⁷). To make a fair comparison between the W partition coefficients of Cottrell et al.³⁰ and the other studies we have used a regression through the Cottrell et al.³⁰ data set which has b set to the value given in thermodynamic tables (as done in the other studies⁶), and have not put any errors on the coefficients a and b . We have kept the error on the valence v as W, unlike the other elements, has a mixed valence state (between 4 and 6), which requires v to be a fitted parameter.

Different elements are sensitive to different model parameters because their partitioning depends in different ways on temperature, pressure, and oxygen fugacity. The inversion

technique is particularly sensitive to the more siderophile elements and to those elements whose uncertainties are smallest, such as Fe, Ni, Co and V. The Fe abundance is best known, and sets the integrated oxygen fugacity. High pressures and an increase in oxygen fugacity are required to simultaneously match the slightly siderophile elements such as V and the more siderophile Ni and Co^{6,29}. Increasing oxygen fugacity also seems to be required to get the correct mantle Nb/Ta ratio⁷. In Figure 1, good fits are seen for all elements, with the exception of Ga. The reason for gallium’s misfit is unclear, but may be due to a poor assessment of the bulk Earth value as it is volatile⁷.

When disequilibrium models are considered (as in Figure 1b) the conditions of differentiation in the embryos are important and must be specified. There is a trade-off between conditions in the embryos and the inferred conditions during accretion. An example is shown in Supplementary Figure 2 where the oxygen fugacity conditions on Earth are plotted as a function of the oxygen fugacity of differentiation in the embryos. If the conditions in the embryos are sufficiently reducing (in this case $\Delta IW = -2.7$), there is no need for an increase in oxygen fugacity during accretion. It should be noted that the misfit (given by (I.1)) also varies as a function of embryo oxygen fugacity, with a value around -0.5 being the best fitting (lowest misfit), and increasing for values lower than this. However, all the embryo values shown in Supplementary Figure 2 still provide good fits to the observations to within the uncertainties. It should be noted that Figure 1 and Supplementary Figure 2 assume all embryos differentiate under the same pressure, temperature, and oxygen fugacity conditions. However, it is likely that this is not the case, and one alternative to having an increase in oxygen fugacity during Earth’s accretion is to have more oxidised material accreting later²⁴.

J Remarks on partially equilibrative plumbing

The $k = 1$ case of the model presented here is exactly the “fully equilibrative plumbing” model first introduced by Harper and Jacobsen⁴⁰. However, the $k < 1$ and $k = 0$ cases are different from the “partially equilibrative plumbing” and “non-equilibrative plumbing” models of Harper and Jacobsen⁴⁰. Partial and non-equilibrative plumbing have metal-silicate equilibration in the embryos occurring at the time of accretion rather than at time 0 as happens here. This can be investigated in the same way, by changing the concentrations in the incoming material from those given in (B.8) to

$$d_{me} = \frac{1}{1 + R_d} \cdot \frac{d_{b0} + p_{b0}(1 - e^{-\lambda t})}{1 - F}, \quad (\text{J.1})$$

$$d_{ce} = \frac{R_d}{1 + R_d} \cdot \frac{d_{b0} + p_{b0}(1 - e^{-\lambda t})}{F}. \quad (\text{J.2})$$

Following through the same calculations as before, the cumulative distribution function associated with the partially equilibrative plumbing model is simply

$$\mathbb{P}(T_d \leq t) = (M(t))^{1+kR_d}, \quad (\text{J.3})$$

which is exactly the same as the distribution of S_d encountered earlier. Hence all the relationships derived for S_d can be applied directly to the partially equilibrative plumbing model. It should be noted that the two stage age t_2 is independent of the degree of equilibration k

for the partially equilibrative plumbing model, $t_2 = t_{2,\text{eq}}$. However, the exponential mean age certainly does depend on k , through

$$e^{-\lambda t_{2,\text{eq}}} = e^{-\lambda t_2} = \frac{\Gamma(2 + kR_d)\Gamma(1 + \lambda\tau_a)}{\Gamma(2 + kR_d + \lambda\tau_a)}. \quad (\text{J.4})$$

For the end-member case of non-equilibrative plumbing ($k = 0$), the above simplifies to

$$t_{2,\text{eq}} = \frac{1}{\lambda} \log(1 + \lambda\tau_a), \quad (\text{J.5})$$

which is the relationship quoted by Jacobsen and Harper⁴¹ (equation (61)) and Harper and Jacobsen⁴⁰ (equation (11)).

K Remarks on the relationship between two stage model ages

The relationship between two stages ages with and without equilibration has also been discussed by Allègre et al.¹⁷, in which it was found that two stage ages $t_2 = 110 - 190$ Myr and degrees of equilibration from 0.86 to 0.94 were needed to obtain overlap between Hf-W and U-Pb. While the inferred ages are broadly in line with those estimated here, the degrees of equilibration are not. The relationship between the two stages ages given by Allègre et al.¹⁷ is

$$1 - e^{-\lambda t_{2,\text{eq}}} = f_d (1 - e^{-\lambda t_2}), \quad (\text{K.1})$$

where symbols have been changed to be compatible with the notation of this manuscript. In Allègre et al.¹⁷, $t_{2,\text{eq}}$ is referred to as the apparent age, and t_2 as the true age, but it should be noted that both ages are examples of model ages. f_d is referred to as the fraction of silicate exchanged. (K.1) should be compared with (C.8), which implies that f_d is related to k by

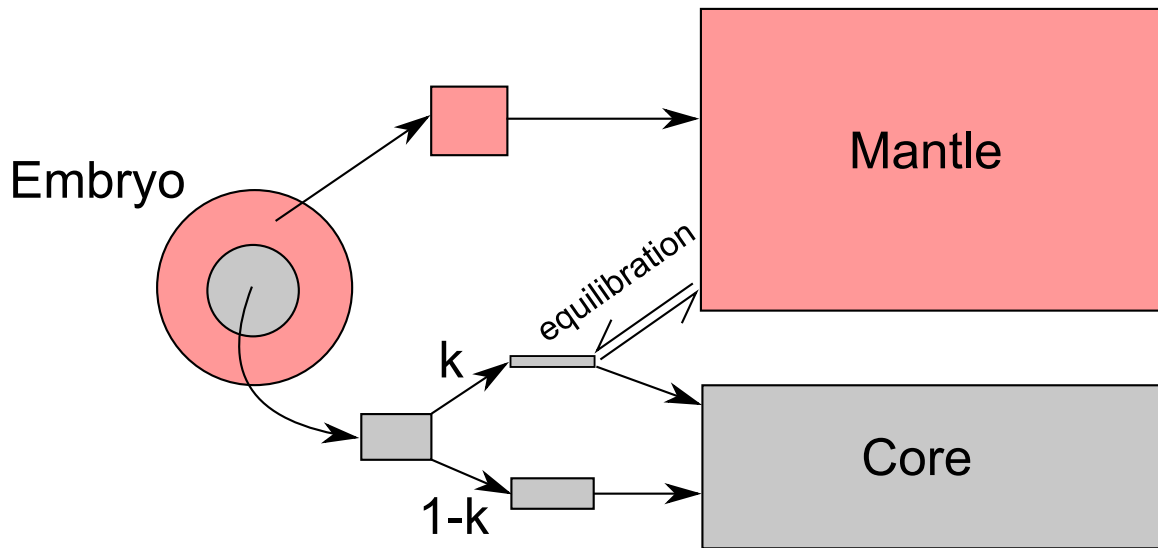
$$f_d = \frac{k(1 + R_d)}{1 + kR_d}. \quad (\text{K.2})$$

The amount of equilibration quoted by Allègre et al.¹⁷ is in terms of f_d rather than the mass fraction k , with 0.86 to 0.94 being values of f_d thought to be consistent with the observations. Allègre et al.¹⁷ assume that f_d is the same for both W and Pb, but as can be seen in (K.2), f_d depends on R_d and thus on the partitioning behaviour of the daughter; likely to be different for W and Pb. The error in Allègre et al.¹⁷ arises from a mistake in using the mixing equation for isotopic ratios in the form $(d/d') = f_d(d/d')_1 + (1 - f_d)(d/d')_2$. The quantity f_d in this equation is not the proportion by mass in which the two quantities mix, but depends on the concentrations of the two substances. The values of f_d quoted by Allègre et al.¹⁷ can be converted to k using (K.2). With a typical value for $R_W = 15$ ($D_W = 33$), the quoted f_d values imply a reequilibration mass fraction k of around 0.28 to 0.49. R_{Pb} is much less well known, but using a value of 6 ($D_{\text{Pb}} = 13$ as used above) implies a reequilibration fraction k of around 0.46 to 0.69. The values of k consistent with both Hf-W and U-Pb estimated here ($k = 0.37 - 0.41$) lie somewhere in the middle of the values one can infer from Allègre et al.¹⁷. Conversely, using the k values here, consistency requires $f_W \approx 0.91$ and $f_{\text{Pb}} \approx 0.81$.

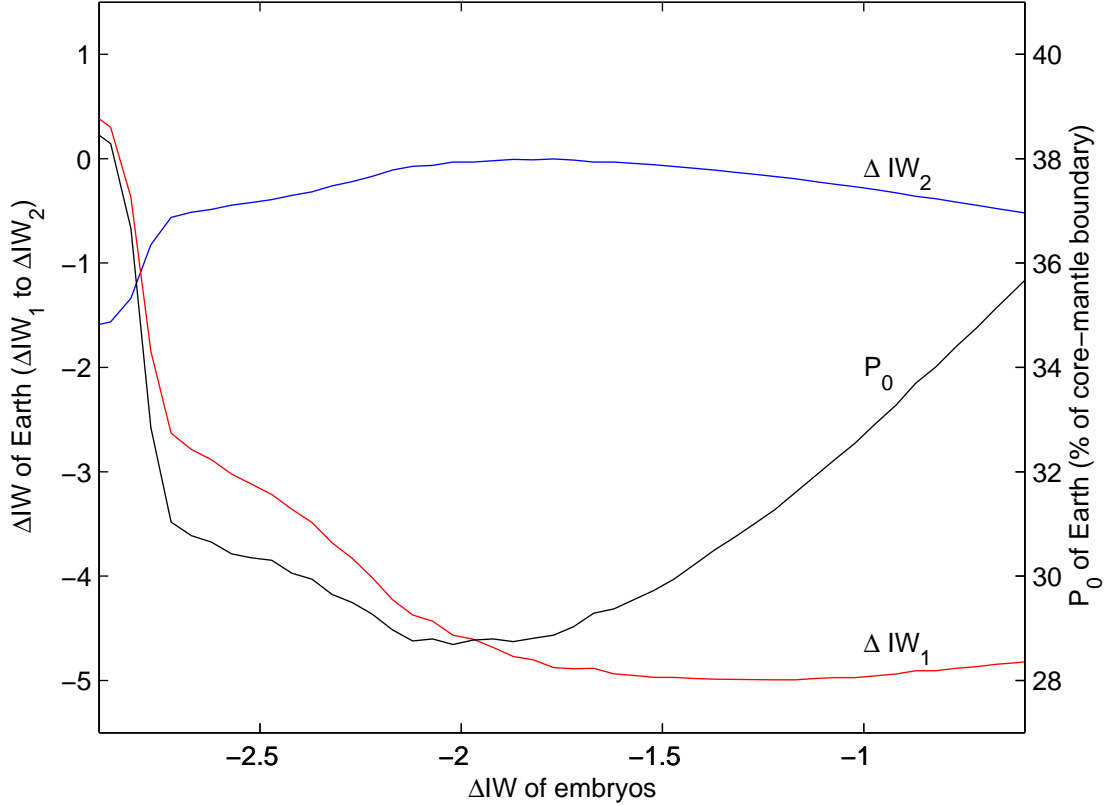
References

- [31] Agnor, C. & Asphaug, E. Accretion efficiency during planetary collisions. *Ap. J.* **613**, L157–L160 (2004).
- [32] Asphaug, E., Agnor, C. B. & Williams, Q. Hit-and-run planetary collisions. *Nature* **439**, 155–160 (2006).
- [33] Rudge, J. F. Mantle pseudo-isochrons revisited. *Earth Planet. Sci. Lett.* **249**, 494–513 (2006).
- [34] Albarède, F. Radiogenic ingrowth in systems with multiple reservoirs: applications to the differentiation of the mantle-crust system. *Earth Planet. Sci. Lett.* **189**, 59–73 (2001).
- [35] Kramers, J. D. & Tolstikhin, I. N. Two terrestrial lead isotope paradoxes, forward transport modeling, core formation and the history of the continental crust. *Chem. Geol.* **139**, 75–110 (1997).
- [36] Murphy, D. T., Kamber, B. S. & Collerson, K. D. A refined solution to the first terrestrial Pb-isotope paradox. *J. Petrol.* **44**, 39–53 (2003).
- [37] Wood, B. J. & Halliday, A. N. Does U-Pb date Earth’s core formation?; How well can Pb isotopes date core formation? (Reply). *Nature* **444**, E2–E3 (2006).
- [38] Bourdon, B., Touboul, M., Caro, G. & Kleine, T. Early differentiation of the Earth and Moon. *Phil. Trans. R. Soc. A* **366**, 4105–4128 (2008).
- [39] Ma, Z. Thermodynamic description for concentrated metallic solutions using interaction parameters. *Metall. Mater. Trans.* **32**, 87–103 (2001).
- [40] Harper, C. L., Jr. & Jacobsen, S. B. Evidence for ^{182}Hf in the early Solar System and constraints on the timescale of terrestrial accretion and core formation. *Geochim. Cosmochim. Acta* **60**, 1131–1153 (1996).
- [41] Jacobsen, S. B. & Harper, C. L., Jr. Accretion and early differentiation history of the Earth based on extinct radionuclides. In *Earth processes: Reading the isotopic code*, 47–74 (AGU Geophysical Monograph 95, 1996).
- [42] Kwon, S.-T., Tilton, G. R. & Grünenfelder, M. H. In *Carbonatites - Genesis and Evolution*, 360–387 (Unwin-Hyman, London, 1989).
- [43] Davies, G. F. Geophysical and isotopic constraints on mantle convection: an interim synthesis. *J. Geophys. Res.* **89**, 6017–6040 (1984).
- [44] Liew, T. C., Milisenda, C. C. & Hofmann, A. W. Isotopic contrasts, chronology of elemental transfers and high-grade metamorphism: the Sri Lanka Highland granulites, and the Lewisian (Scotland) and Nuk (SW Greenland) gneisses. *Int. J. Earth Sci.* **80**, 1437–3262 (1991).
- [45] Galer, S. J. G. & Goldstein, S. L. Depleted mantle lead isotopic evolution using conformable ore leads. *Terra Abstr.* **3**, 485–486 (1991).

- [46] Doe, B. R. & Zartman, R. E. In Barnes, H. L. (ed.) *Geochemistry of Hydrothermal Ore Deposits*, 22–70 (Wiley, New York, 1979).
- [47] Kamber, B. S. & Collerson, K. D. Origin of ocean-island basalts: a new model based on lead and helium isotope systematics. *J. Geophys. Res.* **104**, 25479–25491 (1999).
- [48] Allègre, C. J. & Lewin, E. Chemical structure and history of the Earth: evidence from global non-linear inversion of isotopic data in a three-box model. *Earth Planet. Sci. Lett.* **96**, 61–88 (1989).
- [49] Allègre, C. J., Lewin, E. & Dupré, B. A. A coherent crust-mantle model for the uranium-thorium-lead isotopic system. *Chem. Geol.* **70**, 211–234 (1988).
- [50] Zartman, R. E. & Haines, S. M. The plumbotectonic model for Pb isotopic systematics among major terrestrial reservoirs—A case for bi-directional transport. *Geochim. Cosmochim. Acta* **52**, 1327–1339 (1988).
- [51] Cottrell, E., Walter, M. J. & Walker, D. Erratum to “Metal-silicate partitioning of tungsten at high pressure and temperature: Implications for equilibrium core formation in Earth” [Earth and Planetary Science Letters 281 (2009) 275–287]. *Earth Planet. Sci. Lett.* **289**, 631–634 (2010).
- [52] Allègre, C. J., Poirier, J.-P., Humler, E. & Hofmann, A. W. The chemical composition of the Earth. *Earth Planet. Sci. Lett.* **134**, 515–526 (1995).
- [53] McDonough, W. F. & Sun, S. The composition of the Earth. *Chem. Geol.* **120**, 223–253 (1995).
- [54] McDonough, W. F. Compositional model for the Earth’s core. In *Treatise on Geochemistry* (Elsevier, 2003).



Supplementary Figure 1: A sketch of the box model used throughout this work. Embryo material differentiates into metal and silicate in equilibrium with one another at time 0. Over the course of the accretion, embryo material is added to the Earth. Embryo mantle material is added directly to the Earth's mantle, whereas embryo core material take two routes: a mass fraction k chemically equilibrates with the Earth's mantle as it travels to the core, and the remaining $1 - k$ is added directly to the Earth's core without reequilibration.



Supplementary Figure 2: An example of the trade-off between conditions in the embryos and conditions on Earth in a disequilibrium model ($k = 0.42$). The embryos are assumed to differentiate at pressure $P_{\text{embryo}} = 9$ GPa, temperature $T_{\text{embryo}} = 2700$ K, and oxygen fugacity $\Delta IW_{\text{embryo}}$ as shown on the horizontal axis. The three Earth parameters P_0 (black line), ΔIW_1 (red line), and ΔIW_2 (blue line) which best fit the siderophile element abundances are plotted as a function of $\Delta IW_{\text{embryo}}$. In disequilibrium models, the inferred change in oxygen fugacity is very sensitive to the oxygen fugacity conditions under which the embryos differentiate. In fact, the siderophile element abundances can be explained without an increase in oxygen fugacity over Earth's accretion provided conditions of differentiation in the embryos are sufficiently more reducing than on Earth. In this particular example, $\Delta IW_{\text{embryo}} = -2.8$ and $\Delta IW_{\text{Earth}} = -1.1$ are appropriate values for which an increase in oxygen fugacity during accretion is not required (intersection of the ΔIW_1 and ΔIW_2 curves).

Supplementary Table 1: Input parameters for the Hf-W system¹². These parameters imply an equilibrium two stage model age $t_{2\text{eq}} = 31.0 \pm 4.4$ Myr and equilibrium mean accretion time $\tau_{a,\text{eq}} = 10.6 \pm 0.5$ Myr. The uncertainty is dominated by the uncertainty in mantle $^{180}\text{Hf}/^{184}\text{W}$.

Parameter	Value	Remarks
λ	$(7.78 \pm 0.02) \times 10^{-8} \text{ yr}^{-1}$	Decay constant of ^{182}Hf .
$(^{182}\text{Hf}/^{180}\text{Hf})_{\text{b0}}$	$(9.72 \pm 0.44) \times 10^{-5}$	Initial bulk Earth value. Derived from internal isochron for CAIs.
$(^{180}\text{Hf}/^{184}\text{W})_{\text{b}}$	1.23 ± 0.15	Bulk Earth value, based on CAIs and carbonaceous chondrites.
$(^{180}\text{Hf}/^{184}\text{W})_{\text{m}}$	20.06 ± 5.90	Present day bulk silicate Earth value.
$(^{182}\text{W}/^{184}\text{W})_{\text{b}}$	$0.864699 \pm 0.000012^*$	Present day bulk Earth value (carbonaceous chondrite value).
$(^{182}\text{W}/^{184}\text{W})_{\text{m}}$	$0.864863 \pm 0.000018^*$	Present day bulk silicate Earth value (terrestrial standard value).

* Note that the relative difference for $^{182}\text{W}/^{184}\text{W}$ between bulk silicate Earth and chondrites is better known than the absolute values of $^{182}\text{W}/^{184}\text{W}$ (the difference is 1.9 ± 0.1 in ϵ_{W} units).

Supplementary Table 2: Input parameters for the U-Pb system.

Parameter	Value	Remarks
λ_{238}	$1.551 \times 10^{-10} \text{ yr}^{-1}$	Decay constant of ^{238}U .
λ_{235}	$9.849 \times 10^{-10} \text{ yr}^{-1}$	Decay constant of ^{235}U .
$(^{235}\text{U}/^{238}\text{U})_{\text{b}}$	1/137.88	Present day value.
$(^{206}\text{Pb}/^{204}\text{Pb})_{\text{b0}}$	9.307	Initial bulk Earth value (Canyon Diablo).
$(^{207}\text{Pb}/^{204}\text{Pb})_{\text{b0}}$	10.294	Initial bulk Earth value (Canyon Diablo).

Supplementary Table 3: Estimates of bulk silicate Earth lead isotopic composition with calculated μ and model ages (based on Table 1 of Halliday 2004¹⁵, but with slightly different model assumptions). μ is the present day $^{238}\text{U}/^{204}\text{Pb}$ value. Calculated values assume a constant partition coefficient $D_{\text{Pb}} = 13^{28}$ and an initial time of 4567 Myr before present. The model ages are not well constrained, ranging from $t_{2,\text{eq}} = 53.5 - 171.0$ Myr and $\tau_{a,\text{eq}} = 20.7 - 67.3$ Myr with this assumed value of the partition coefficient.

Reference	$(^{206}\text{Pb}/^{204}\text{Pb})_{\text{m}}$	$(^{207}\text{Pb}/^{204}\text{Pb})_{\text{m}}$	μ_b	μ_m	$t_{2,\text{eq}}$ (Myr)	$\tau_{a,\text{eq}}$ (Myr)
Kramers and Tolstikhin 1997 ³⁵	17.440	15.160	1.13	8.05	74.7	29.0
Kwon et al. 1989 ⁴²	17.822	15.445	1.18	8.38	55.9	21.6
Davies 1984 ⁴³	17.830	15.457	1.18	8.39	53.5	20.7
Liew et al. 1991 ⁴⁴	17.920	15.470	1.20	8.51	67.2	26.0
Murphy et al. 2003 ³⁶	18.070	15.540	1.22	8.67	73.7	28.6
Galer and Goldstein 1991 ⁴⁵	18.110	15.617	1.22	8.67	56.6	21.9
Doe and Zartman 1979 ⁴⁶	18.252	15.476	1.26	8.98	130.5	51.0
Kamber and Collerson 1999 ⁴⁷	18.270	15.600	1.25	8.91	93.0	36.2
Allègre and Lewin 1989 ⁴⁸	18.340	15.551	1.27	9.05	122.5	47.9
Allègre et al. 1988 ⁴⁹	18.400	15.580	1.28	9.12	124.4	48.6
Zartman and Haines 1988 ⁵⁰	18.619	15.565	1.33	9.45	171.0	67.3

Supplementary Table 4: Coefficients used in the partition coefficient parametrisation (G.4). Values in brackets are the 1 standard deviation error on the regression coefficients. $\gamma_M^{\text{net}}(T_0)$ are the C-unsaturated activity coefficients calculated at a reference temperature of $T_0 = 1873$ K using an interaction parameter approach⁷ (not used for Ti, Zn, or Pb). P coefficients from⁶ are based on unpublished data by M. Walter. Uncertainties on the regression coefficients are not available for P or Pb.

	v	a	b (K)	c (K GPa^{-1})	d	$\gamma_M^{\text{net}}(T_0)$	reference
Mn	2	-0.02	-5600	38 (6)	0.036 (0.010)	0.6473	Corgne et al. 2008 ⁷
Ni	2	0.50	3100	-78 (5)	-0.073 (0.015)	0.6819	Corgne et al. 2008 ⁷
Cr	2	0.09	-2845 (461)	-20 (10)	0.000 (0.013)	0.7705	Corgne et al. 2008 ⁷
Ga	3	3.50	-4800	-126 (36)	-0.97 (0.15)	0.8762	Corgne et al. 2008 ⁷
Si	4	2.97	-21800	-11 (33)	-0.24 (0.11)	0.0077	Corgne et al. 2008 ⁷
Nb	5	4.09	-15500	-166 (31)	-0.75 (0.16)	0.1107	Corgne et al. 2008 ⁷
Ta	5	7.74	-20000	-264 (81)	-1.69 (0.53)	0.1029	Corgne et al. 2008 ⁷
Ti	4	3.46	-19000	-42 (52)	-0.11 (0.16)	1.0000	Corgne et al. 2008 ⁷
Cu	1	0.30	2300	-37 (45)	0.14 (0.17)	10.9980	Corgne et al. 2008 ⁷
Zn	2	-1.11	600	-23 (102)	-0.21 (0.24)	1.0000	Corgne et al. 2008 ⁷
V	3	0.855	-8548	-62 (19)	-0.101 (0.029)	0.1076	Wood et al. 2008 ²⁹
Co	2	0.01	2511	-45 (11)	0	0.4790	Wade and Wood 2005 ⁶
P	5	0.64	-1593	-74.95	0	4.2805	Wade and Wood 2005 ⁶
W	4.52 (0.52)	3.2	-1605	-115 (15)	-0.85 (0.07)	0.9411	Cottrell et al 2009 ^{30,51}
Pb	2	0.788	-2436	0	0	1.0000	Wood et al. 2008 ²⁸
Fe	2	0	0	0	0	0.8762	

Supplementary Table 5: Effective partition coefficients inferred from present day core/mantle concentrations, $D^{\text{obs}} = c_{\text{c}}^{\text{obs}}/c_{\text{m}}^{\text{obs}}$. First column shows $\log_{10} D_{\text{obs}}$ with a 1 standard deviation error in brackets. The 2σ range for D_{obs} that results is shown in the second column. Asterixes (*) denote volatile elements, for which estimates of bulk Earth composition are much more uncertain. Estimates are based on those used by Corgne et al.⁷ and Wade and Wood⁶ (in turn based on⁵²⁻⁵⁴) with the exception of W which is based on¹². The volatile and only moderately siderophile elements Zn and Ga have very uncertain abundances. Ti is normally regarded as a refractory lithophile element, and thus its concentration in the core is usually estimated to be zero.

	$\log_{10} D^{\text{obs}}$	2σ interval for D^{obs}
W	1.513 (0.077)	23-46
Ni	1.418 (0.017)	24-28
P*	1.398 (0.140)	13-48
Co	1.381 (0.013)	23-26
Pb	1.159 (0.118)	8-25
Fe	1.136	13.66
Cu*	0.801 (0.099)	4-10
V	0.262 (0.042)	1.5-2.2
Cr*	0.195 (0.175)	0.7-3.5
Mn*	-0.155 (0.274)	0.2-2.5
Nb	-0.276 (0.211)	0.2-1.4
Ta	-0.611 (0.195)	0.1-0.6
Si*	-0.728 (0.136)	0.10-0.35
Zn*	-0.824 (0.301)	0-0.6
Ga*	-1.000 (0.301)	0-0.4
Ti	$-\infty$	0

Supplementary Table 6: Table of variables

a, b, c, d, v	coefficients used in partition coefficient parametrisation ((G.5) and Supplementary Table 4)
c_b	concentration of chemical species in the bulk Earth
c_c	concentration of chemical species in the Earth's core
c_{c0}	initial concentration of chemical species in the Earth's core (c_c at $t = 0$)
c_{ce}	concentration of chemical species in the core of the embryos
c_m	concentration of chemical species in the Earth's mantle
c_{me}	concentration of chemical species in the mantle of the embryos
d	daughter isotope, e.g. ^{182}W
d'	reference isotope, e.g. ^{184}W
D	partition coefficient by mass
D^*	partition coefficient by mole
D^{model}	c_c/c_m from model calculations
D^{obs}	c_c/c_m from observed abundances (Supplementary Table 5)
F	mass fraction of Earth's core (0.323)
k	mass fraction of metal that chemically equilibrates during accretion
$M(t)$	fraction of Earth accreted at time t
N	molar ratio of non-bridging oxygens to tetrahedral cations in the silicate melt
p	parent isotope, e.g. ^{182}Hf
p'	reference isotope, e.g. ^{180}Hf
P	pressure
R	$= FD/(1 - F)$
S_d	random variable defined by (C.1)
t	time since beginning of solar system
t_2	two stage model age
$t_{2,\text{eq}}$	two stage model age, assuming full equilibration ($k = 1$)
T	temperature
T_d	random variable defined by (B.13)
α	time scale parameter of Weibull distribution
β	shape parameter of Weibull distribution
γ	activity coefficient
ΔIW	oxygen fugacity relative to the iron-wüstite buffer in \log_{10} units
λ	decay constant
μ	$^{238}\text{U}/^{204}\text{Pb}$ isotopic ratio corrected for radioactive decay
σ	standard deviation
τ_a	exponential model age (mean age and time of 63% accretion)
$\tau_{a,\text{eq}}$	exponential model age, assuming full equilibration ($k = 1$)
